THESIS FOR DEGREE OF DOCTOR OF PHILOSOPHY

Experimental studies of ice particle Formation Studies with Tropospheric Relevance

Erik Svensson

The thesis will be defended in English
on Friday the 28th of Nov, 2008, at 10:15 in room 10:an in the Chemistry Building
University of Gothenburg and Chalmers University of Technology

Faculty opponent is Professor John Wettlaufer
Nordic Institute for Theoretical Physics
Stockholm, Sweden

UNIVERSITY OF GOTHENBURG

Department of Chemistry, Atmospheric Science
University of Gothenburg
Sweden, 2008

List of papers

This thesis is based on the work presented in the following papers:

I. Svensson, E.A., Badiei, S., Hallquist, M., Pettersson, J.B.C, “Freezing of evaporating oxalic acid solution droplets”, Submitted to *Journal of Physical Chemistry A*.

II. Svensson, E. A, Pettersson J. B. C., “Evaporation freezing of water droplets: influence of initial oxalic acid concentration”, Manuscript for *Geophysical Research Letters*.

III. Svensson, E. A., Delval, C., von Hessberg, P., Johnson, M. S., Pettersson, J. B. C, “Freezing of water droplets colliding with kaolinite particles”, Submitted to *Atmospheric Chemistry and Physics*.

IV. Olofson, K. G. F., Svensson, E. A., Witt, G., Pettersson, J. B. C., “Arctic aerosol and clouds studied by bistatic lidar technique”, Submitted to *Journal of Geophysical Research: Atmospheres*.

V. Romero Lejonthun, L. S. E., Svensson, E. A., Andersson, P. U. and Pettersson, J. B. C., “Formation of adsorbed layers by deposition of dinitrogen pentoxide, nitric acid and water on graphite”, Submitted to *Journal of Physical Chemistry C*.

Table of contents

1. Introduction

The atmosphere of the Earth is the gas layer which surrounds the liquid and solid surface. Without it, our planet would be different from the way we know it. It would, basically, be a quite nasty place. The surface would be exposed to ionizing ultraviolet radiation from the sun. The global mean temperature would be lower and the variations in temperature would be extreme.

The gases that constitute the atmosphere are kept from escaping into space by gravity. The pressure decreases successively when ascending from the ground and there is no definite boundary between the atmosphere and space. It is, however, generally considered that the atmosphere ends at about 100-120 km above the ground. A comparison with the Earth's radius of more than 6000 km makes one realize how thin the gas layer really is. Pictures, such as the "Blue Marble" taken from Apollo 17, gives a visualization of the atmosphere.

Beginning at the very end of the 19th century, scientists started to realize that human activity could alter the atmosphere in a substantial way (Weart, 2007). Burning of fossil fuels releases carbon in the form of carbon dioxide into the atmosphere at a rate which natural processes cannot compensate for. Arrhenius (1896) made the first attempt to quantify the effect of increased atmospheric carbon dioxide on climate. Even though Arrhenius´ calculations were shown to be erroneous, the numbers are still in line with present estimates.

In contrast to the relative simplicity of well-mixed greenhouse gases, such as carbon dioxide and methane, water vapor has a highly dynamic behavior in the atmosphere. Water on the ground evaporates and humidifies the air close to the ground. When the humid air is lifted it cools causing the water vapor to condense on aerosol particles. A cloud is formed, whose properties depend on the conditions under which it is formed. Clouds are not only important for the radiative balance, they can also be beautiful or funny watching (http://cloudappreciationsociety.org/). Eventually, the water in the atmosphere will fall to the ground, either as frozen or liquid.

Understanding how the climate on Earth works is a huge task. There are obviously no possibilities of doing controlled full-scale experiments. Hence, we are restricted to use experimental results to make models and compare with observational results. Discrepancies between models and observations can highlight areas where more research is needed. In this thesis, I will present the small, yet important, contribution I have made to the understanding of how the atmosphere works. My work has been focused on ice formation in clouds.

This thesis is based on five appended papers on four subjects:

- Freezing of evaporating oxalic acid solution droplets (papers I & II).
- Freezing of pure water droplets colliding with kaolinite dust particles (paper III).
- Lidar studies of Arctic clouds and aerosol (paper IV).
- Interactions between N_2O_5, HNO_3 and graphite and the effects of N_2O_5 on ice formation onto graphite (paper V).

In chapter 2, I will give some theoretical background to the issues discussed. The different experimental methods are described in chapter 3 and the results are summarized in chapter 4. In chapter 5, I will discuss the implications of my work and the future work that can be recommended in order to continue the research.

2. Background

2.1 Overview of the climate system

Global climate change poses a serious threat to the continued development of human society (IPCC, 2007). Global mean temperature have risen by about 0.7 K since the middle of the 19th century and is projected to continue rising due to increasing levels of greenhouse gases (GHGs), mainly carbon dioxide. Mountain glaciers are shrinking, which will cause water shortage for people depending on melt water. Precipitation patterns are changing and sea levels are rising. Heat waves are getting more intense and tropical cyclones may become more intense even though the link is not clear.

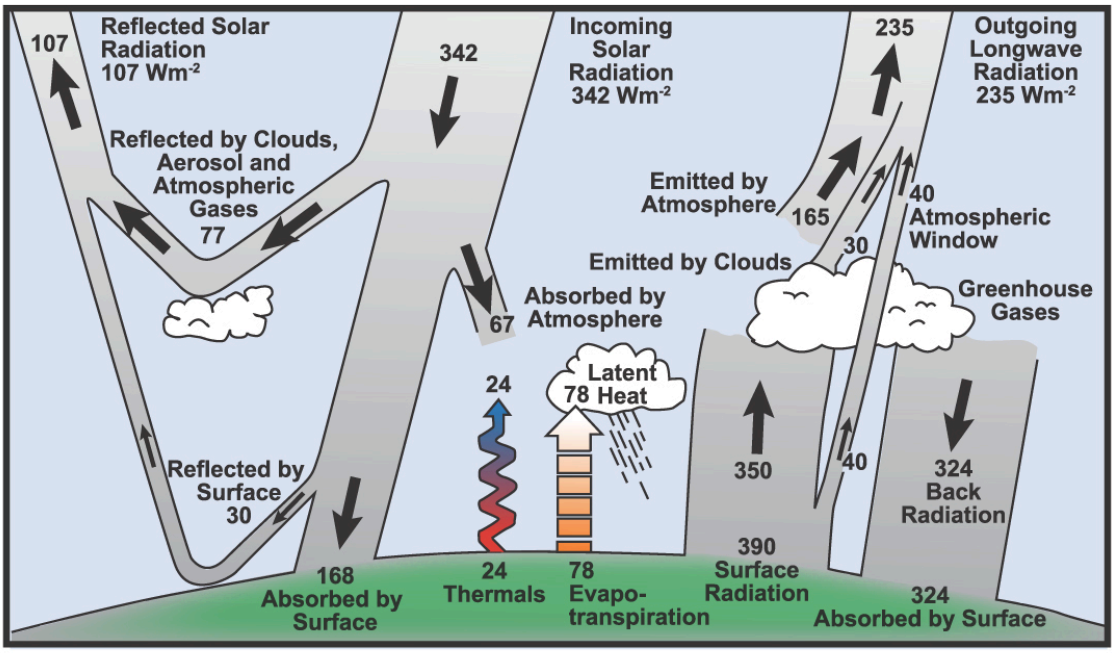

Figure 1. *Earth's globally and annually averaged energy balance according to IPCC (AR4, FAQ1.1 fig. 1, 2007).*

Science clearly attributes the major part of observed global climate change to the increases in GHG concentrations. However, the uncertainties in projections for the future are large. The temperature of the Earth is basically determined by the energy flux; short wave solar radiation heats the planetary surface, long wave infrared radiation sends energy into space (Harvey, 2002). The global average surface temperature is estimately 287 K. Figure 1 shows an overview of the heat fluxes on Earth. An important equation is used to describe the changes in global mean temperature ΔT:

$$\Delta T = \lambda \cdot \Delta F \qquad (1)$$

where ΔF is the change in the mean net radiative flux in W/m^2 and λ is a parameter called the climate sensitivity. ΔF, also known as radiative forcing (RF), can be caused by several independent factors, such as variations in incoming solar flux, changes in surface reflectivity and GHG concentrations. The IPCC estimates of the RFs for the most important factors are shown in figure 2.

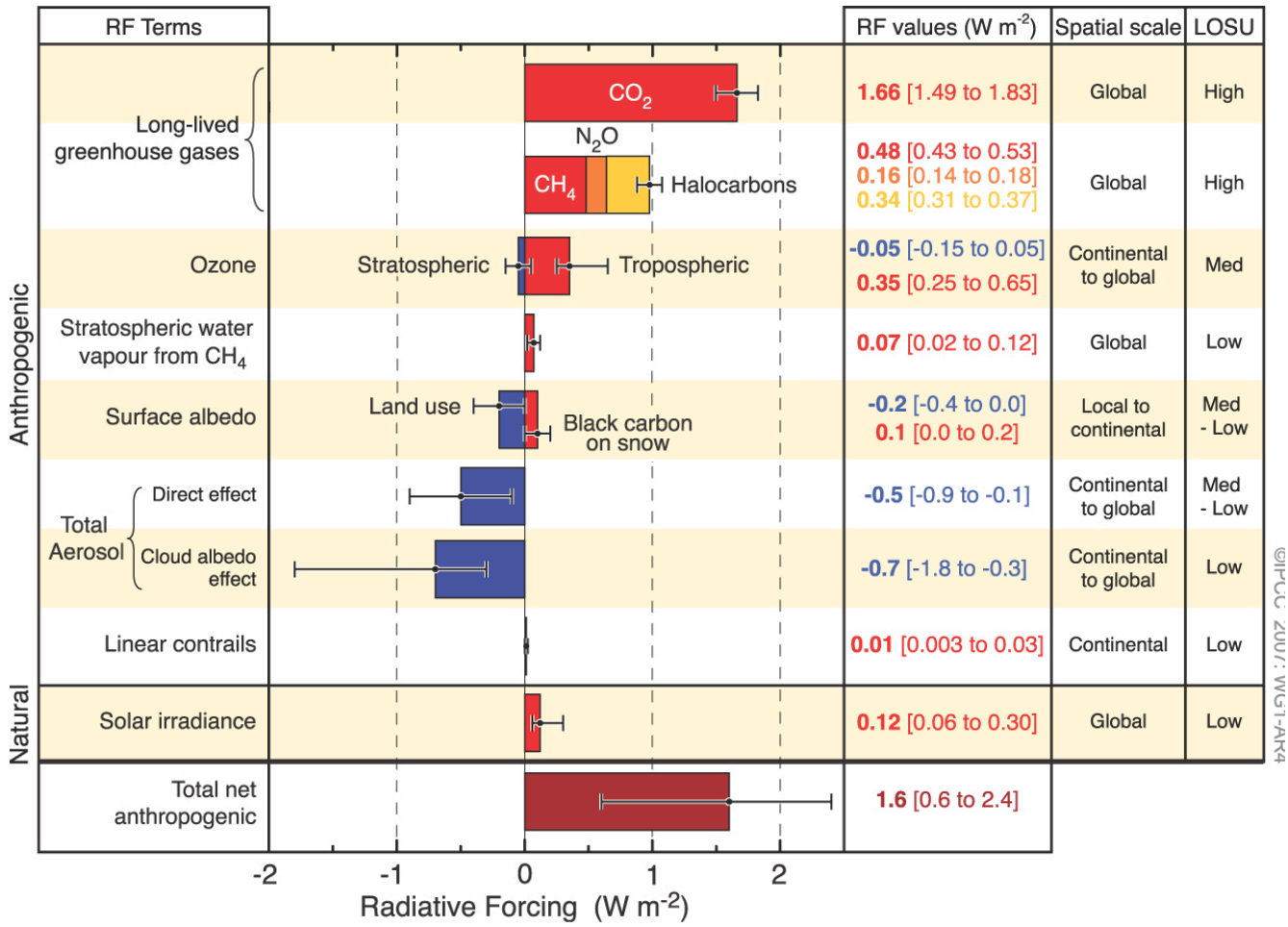

Figure 2. *Estimated radiative forcing since 1750 (IPCC, AR4, FAQ2.1, fig. 2, 2007).*

GHGs absorb some of the outgoing infrared radiation from the surface without absorbing incoming light. Hence, increasing GHG concentrations will cause a radiative imbalance heating the surface and atmosphere of the Earth. This heating causes an increased emission of heat radiation until the radiative balance is restored. The climate sensitivity, λ, couples the RF with the temperature change. Assuming that only the temperature changes, the climate sensitivity can be estimated by Stefan-Boltzmann´s law to be about 1 K for the RF (~3.7 W/m^2) associated with a doubling of the carbon dioxide concentration from the pre-industrial level of 280 parts per million (ppm) to 560 ppm (Harvey, 2002). The current value is about 385 ppm.

In reality several other factors change when the temperature is changed. Some of these changes themselves cause radiative imbalances. Hence, these factors act as feedbacks, which can either amplify or damp the temperature change. For example, the water vapor content increases with increasing temperature. Water vapor is the most important GHG in the atmosphere, causing approximately 60% of the natural greenhouse effect (Karl and Trenberth, 2003). The increased water vapor content will amplify the initial warming, an effect which has been observed by satellite measurements (Held, 2006).

The real value of the climate sensitivity thus depends on the feedbacks (Roe and Baker, 2007).

Estimates from climate models and empirical studies indicate that λ is within the range 2 – 4.5 K for a doubling of the CO_2 concentration with a best estimate of 3 K (IPCC, 2007). The major uncertainty in both models and empirical estimates is due to aerosols, i.e. particles suspended in the atmosphere. The level of understanding of aerosol processes and their effect on the climate system is low, as illustrated in figure 2. The RF from the well-mixed GHGs is quantified with good precision, while on the other hand the effects of the aerosol are uncertain.

2.2 Aerosols, clouds and climate

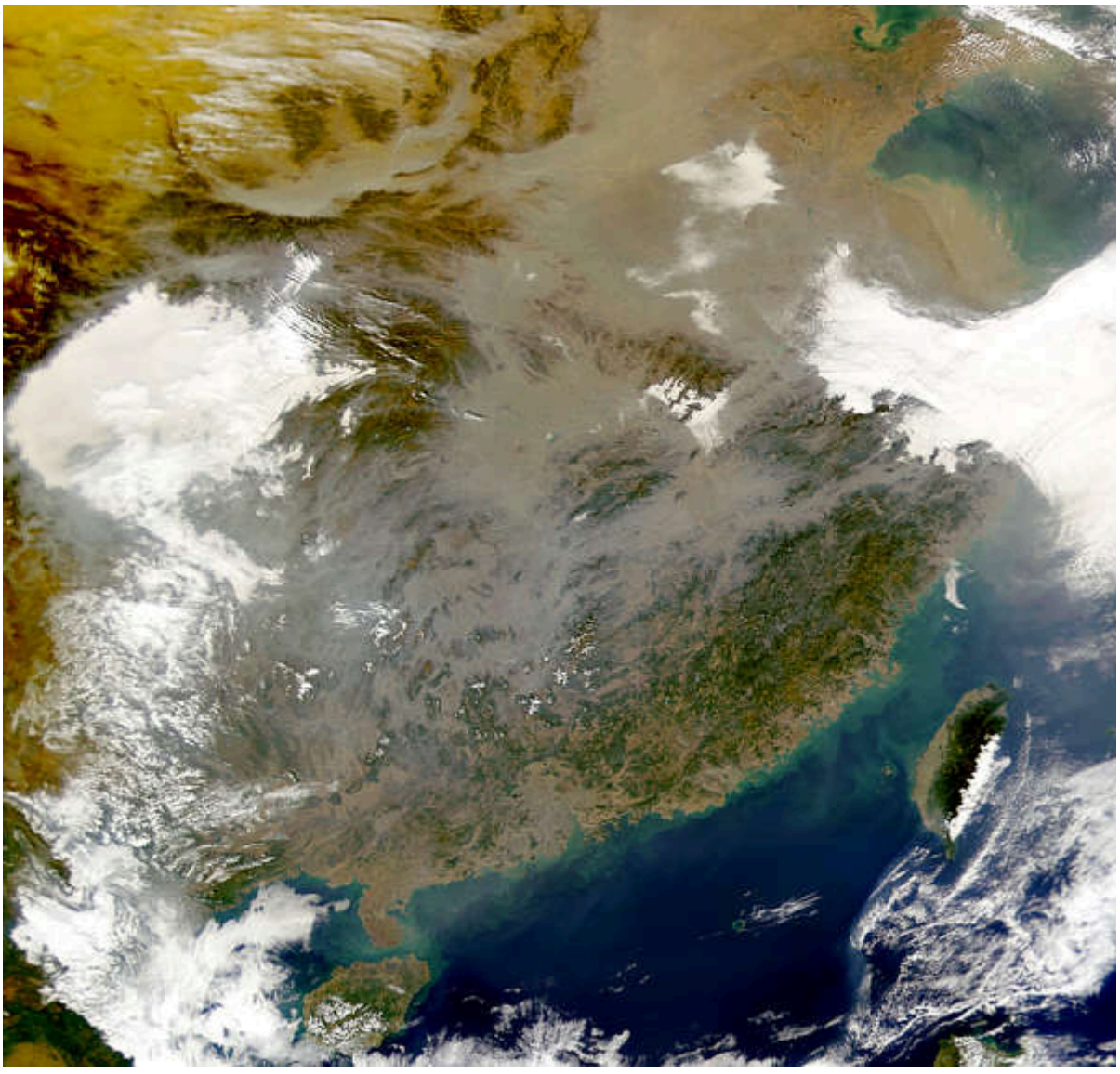

Figure 3. *Satellite image of particulate pollution over eastern China. Even though the aerosol is grayish, it is lighter than the ground and thus has a cooling effect. Picture courtesy of NASA (http://visibleearth.nasa.gov/).*

The atmospheric aerosol interacts in very complex ways with the climate system. Primarily, particles, which can be solid, liquid or a mixture between them, scatter and absorb light. The size distribution, shape and refractive index of the aerosol determine the optical behavior (Mishchenko et al., 2002). Additional factors such as the time of day and altitude matter when estimating the effects. As shown in figure 2 the total RF from anthropogenically induced changes in aerosol properties is believed to be negative, i.e. cooling which can be visualized in figure 3. Hence anthropogenically emitted particles may be masking the global warming.

Furthermore, the formation of clouds requires aerosol particles which act as *cloud condensation nuclei* (CCN). The air would otherwise stay highly supersaturated with respect to water vapor. The CCN number concentration is a crucial parameter for the development of a cloud. A high CCN concentration will cause the cloud to be composed of many small droplets instead of a few large. The cloud becomes more optically dense and less light can pass through it (Lohmann and Feichter, 2005). This is often referred to as the *Twomey effect*. In addition, smaller but more numerous cloud droplets in a cloud reduces the precipitation efficiency. This prolongs the cloud lifetime and reduces the amount of light reaching the surface. In a recent review by Lohmann and Feichter (2005) the aerosol climatic effects are assessed. Figure 4 illustrates the most important aerosol-cloud climatic effects (IPCC, 2008). There is no simple relationship between the amount of clouds and the heating or cooling of the ground. Depending on factors such as cloud altitude and time of day, clouds can be either cooling or heating.

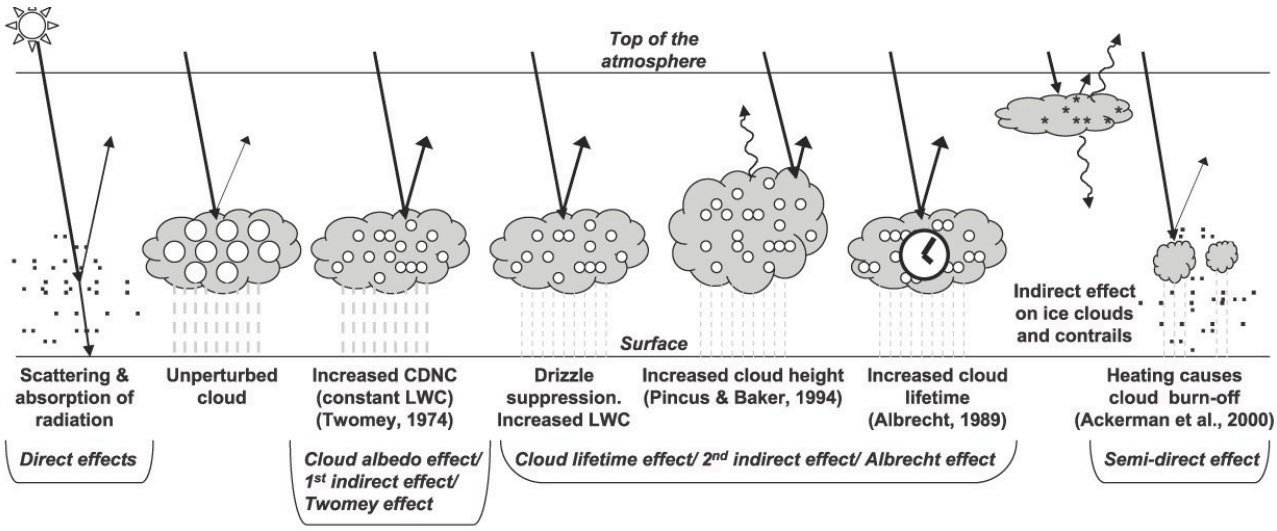

***Figure 4**. Illustration of cloud-aerosol processes. (IPCC, AR4 fig. 2.10, 2007)*

2.3 Freezing processes

Freezing of cloud droplets plays a vital role in the climatic system due to thermodynamic effects. Water ice has a lower equilibrium vapour pressure than supercooled water at the same temperature. Hence, in a mixed-phase cloud, the ice particles will effectively "steal" mass from the water droplets. This is called the *Bergeron-Wegener-Findeisen process* (Pruppacher and Klett, 1997) and may induce precipitation from clouds. The ice particles gain mass and start to descend, which causes collisions with water droplets. This in turn increases the mass of the ice particles causing the particles to fall towards

the ground. Freezing of cloud droplets may thus can remove water from a cloud and decrease its lifetime. Freezing does however not occur spontaneously in cloud droplets at temperatures above about 240 K (-33 °C)(Cantrell and Heymsfield, 2005). It is difficult for the liquid water in a droplet to organize in ice-like structures by itself, so called *homogeneous* freezing. In liquid water, molecules continuously arrange in small clusters which quickly disarrange. However, at low temperatures a cluster may grow above some critical limit and become thermodynamically stable, and the whole water volume will then freeze. The probability of homogeneous freezing can be described using an Arrhenius-type expression with a nucleation rate constant J (the number of freezing events per second and cubic centimetre),

$$J = J_0 e^{\frac{-\Delta E}{kT}} \qquad (2)$$

where J_0 is a prefactor, k is Boltzmann's constant, T is the temperature, and ΔE is the height of the energy barrier for the formation of a sufficiently large ice-like cluster (Pruppacher and Klett, 1997, Cantrell and Heymsfield, 2005). Aqueous solutions generally have even lower freezing temperatures. A quite general theory has been developed which describes the freezing rates of aqueous solutions in terms of the *water activity*, i.e. the equilibrium water vapor pressure compared to that of pure water (Koop et al., 2000).

There is a discussion within the scientific community on where the homogeneous freezing preferably starts within a droplet. It has been claimed (e.g. Tabazadeh et al. 2002a, 2002b, Djikaev et al., 2002, Vrbka and Jungwirth, 2006, Djikaev, 2008) that the surface or its vicinity is the main homogeneous nucleation site, at least for sub-micrometer droplets. Duft and Leisner (2004) showed that for droplets in the micrometer size range, the freezing is dependent on the droplet volume rather than the surface area. The surface nucleation hypothesis has also been contrasted by several other studies (e.g. Knopf et al., 2002 and Stretzer et al., 2006). Recently, the analysis by Tabazadeh (2002a, 2002b) has been suggested to be based on an erroneous approximation in the data analysis (Sigbjörnsson and Signorell, 2008).

Freezing can also be induced *heterogeneously* while water interacts with a solid surface. The surface structure of the solid helps aligning the molecules in an ice-like structure. In cloud droplets, the surface is provided by an insoluble particle, the ice nucleus (IN). Mineral dust and soot particles are considered to make up a large portion of IN in the atmosphere (Cantrell and Heymsfield, 2005). There are traditionally four modes of freezing, which are illustrated in figure 5. These processes occur under different atmospheric conditions. Immersion freezing (mode A) occurs when a droplet, which was formed onto a solid particle under temperatures too high for freezing, gets cooled and freezes. If instead the temperature is low and the RH increases, liquid water may condense on the nucleus. At some stage of the droplet growth, the water freezes. This is the condensation freezing (mode B) in figure 5. Dry, solid particles may collide with pre-existing supercooled water droplets, and induce freezing (contact nucleation, mode C). The last process is the deposition freezing, where ice is formed directly from vapor phase (mode D). Comparing the immersion and contact freezing modes (modes A and C in figure 5) the freezing generally occurs at significantly higher temperatures in the contact mode for each type of particle (e.g. Pitter and Pruppacher, 1973, von Blohn, 2005 and Pruppacher and Klett, 1997). Currently there is no unifying theory to explain this behaviour, but a growing body of evidence indicates that the three phase-lines of solid particles intersecting a water surface is a preferential site of heterogeneous ice nucleation (Shaw et al., 2005, Durant and Shaw, 2005, Suzuki et al, 2007a and

2007b).

Shaw (2005) and Durant and Shaw (2005) showed experimentally that the contact freezing could also be induced from inside a droplet. In one experiment, a pure water drop containing avolcanic ash particle was first cooled until it froze, then heated until it melted. This procedure was repeated and the freezing temperature was recorded each time. As the droplet evaporated, the particle eventually interfered with the surface of the water droplet from the inside. When this happened, the freezing occurred at higher temperatures than in the previous freezing cycles. Comparing in-situ studies of a wave cloud with parcel modelling, Cotton and Field (2002) found that freezing occurred during evaporation of the cloud droplets.

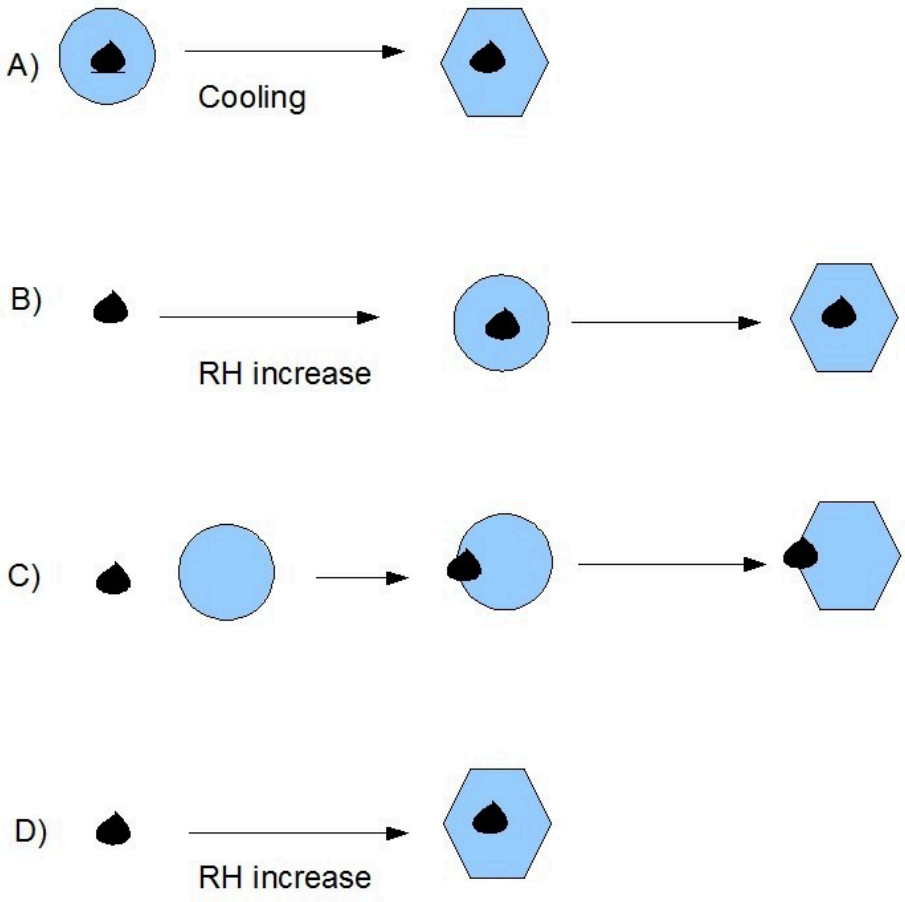

Figure 5. *Cartoon showing the modes of heterogeneous freezing. A) Immersion freezing: An immersed IN activates as the temperature decreases. B) Condensation freezing: A particle acts as CCN and as the droplet grows it eventually freezes. C) Contact freezing: An IN collides with a water droplet and induces freezing. D) Deposition freezing: Ice forms directly from vapor phase onto the particle.*

2.4 Light scattering

2.4.1 Electrodynamics and light

Light, being an electromagnetic phenomenon, is fundamentally governed by Maxwell's famous equations (Mishchenko et al. 2002, Bohren and Huffman, 1999, Jackson, 1999):

$$\nabla \cdot \boldsymbol{D} = \rho \tag{3}$$

$$\nabla \times \boldsymbol{E} = -\frac{\partial \boldsymbol{B}}{\partial t} \tag{4}$$

$$\nabla \cdot \boldsymbol{B} = 0 \tag{5}$$

$$\nabla \times \boldsymbol{H} = \boldsymbol{J} + \frac{\partial \boldsymbol{D}}{\partial t} \tag{6}$$

where t is time, $\boldsymbol{E}$ and $\boldsymbol{H}$ the electric and magnetic fields respectively, $\boldsymbol{B}$ the magnetic induction, $\boldsymbol{D}$ the electric displacement and ρ and $\boldsymbol{J}$ the charge density and current density, respectively. In uniform isotropic linear media $\boldsymbol{D}=\varepsilon\boldsymbol{E}$ and $\boldsymbol{B}=\mu\boldsymbol{H}$ where ε and μ are the permittivity and permeability, respectively. Combining Maxwell´s equations, wave equations can be derived:

$$\nabla^2 \boldsymbol{E} + \mu\epsilon \frac{\partial^2 \boldsymbol{E}}{\partial t^2} = 0 \tag{7}$$

$$\nabla^2 \boldsymbol{B} + \mu\epsilon \frac{\partial^2 \boldsymbol{B}}{\partial t^2} = 0 \tag{8}$$

Essentially, this means that the $\boldsymbol{E}$ and $\boldsymbol{B}$ fields couple and can, in vacuum, move any distance without charges or currents present. Assuming harmonic time dependence $e^{-i\omega t}$ eq. (7 & 8) can be written as

$$\nabla^2 \boldsymbol{E} + \mu\epsilon\omega^2 \boldsymbol{E} = 0 \tag{9}$$

$$\nabla^2 \boldsymbol{B} + \mu\epsilon\omega^2 \boldsymbol{B} = 0 \tag{10}$$

One important solution to Eqs. 8 and 9 is the *plane wave* where the fields are described by:

$$\boldsymbol{E}(\boldsymbol{x}, t) = E_0 \mathrm{e}^{ik\boldsymbol{n}\cdot\boldsymbol{x} - i\omega t} \tag{11}$$

$$\boldsymbol{B}(\boldsymbol{x}, t) = B_0 \mathrm{e}^{ik\boldsymbol{n}\cdot\boldsymbol{x} - i\omega t} \tag{12}$$

where $\boldsymbol{x}$ is the position and $\boldsymbol{n}$ the vector of the wave propagation direction. E_0 is the amplitude of the waves. The components can be described alone, and usually the E-component is used.

2.4.2 Polarization

The wave described in Equation 11is *linearly polarized.* This means that when looking in the direction of the wave, the field propagates in only one direction, which can be defined by a two-dimensional vector $\boldsymbol{\varepsilon}_1$. The wave can also have a component in the direction perpendicular to $\boldsymbol{\varepsilon}_1$, $\boldsymbol{\varepsilon}_2$. Then, the total wave can be written as:

$$\boldsymbol{E}(\boldsymbol{x},t)=(E_1\boldsymbol{\epsilon}_1+E_2\boldsymbol{\epsilon}_2)\mathrm{e}^{ik\boldsymbol{n}\cdot\boldsymbol{x}-i\omega t} \tag{13}$$

where E_1 and E_2 are amplitudes, which are generally complex to allow phase differences. The polarization state of the wave is often described by the *Stokes vector*:

$$\boldsymbol{I}=\begin{bmatrix} I \\ Q \\ U \\ V \end{bmatrix}=\frac{1}{2}\sqrt{\frac{\epsilon}{\mu}}\begin{bmatrix} |\boldsymbol{\epsilon}_1\cdot\boldsymbol{E}|^2+|\boldsymbol{\epsilon}_1\cdot\boldsymbol{E}|^2 \\ |\boldsymbol{\epsilon}_1\cdot\boldsymbol{E}|^2-|\boldsymbol{\epsilon}_1\cdot\boldsymbol{E}|^2 \\ 2\,\mathrm{Re}\left[(\boldsymbol{\epsilon}_1\cdot\boldsymbol{E})*(\boldsymbol{\epsilon}_2\cdot\boldsymbol{E})\right] \\ 2\,\mathrm{Im}\left[(\boldsymbol{\epsilon}_1\cdot\boldsymbol{E})*(\boldsymbol{\epsilon}_2\cdot\boldsymbol{E})\right] \end{bmatrix} \tag{14}$$

The components *I, Q, U* and *V* have the great advantage of being observables. With proper equipment it is possible to observe them separately. *I* is the total intensity of the light, while *Q*, *U* and *V* describe the intensity in different polarization states, which in general is elliptic in monochromatic light. The parameters are explained in figure 6.

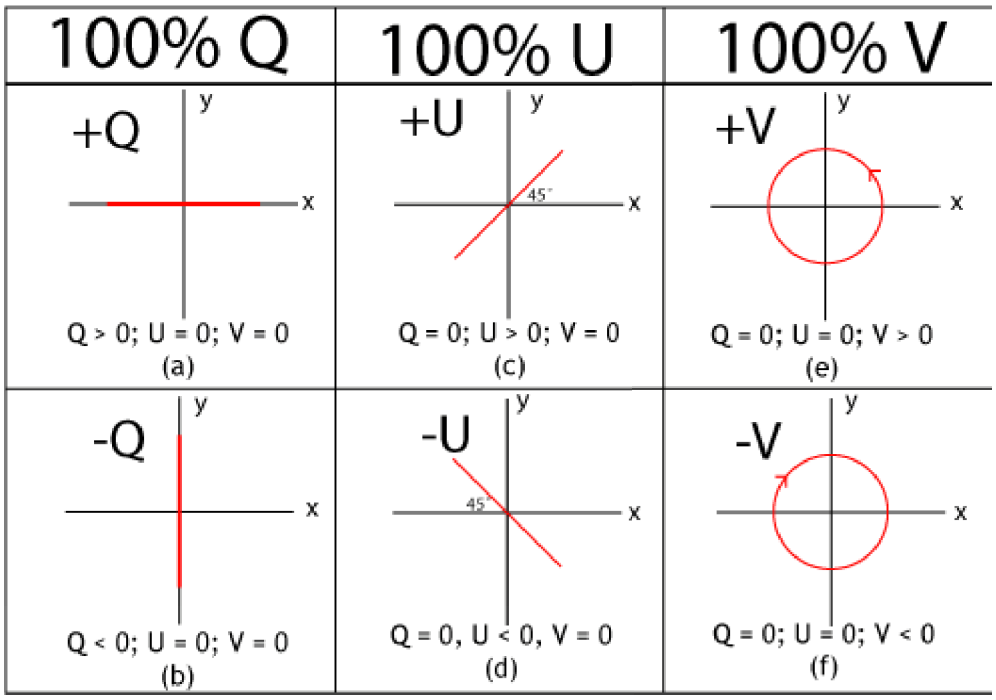

***Figure 6**. Some special cases of the Stokes parameters. In general, Q, U and V can be non-zero producing an elliptic polarization.*

For monochromatic light the Stokes parameters are not completely independent: $\sqrt{Q^2+U^2+V^2}=I$, but

for non-monochromatic light $\sqrt{Q^2+U^2+V^2} < I$.

2.4.3 Light Scattering by particles

Since the Stokes vector provides a sufficient description of the light, scattering can be mathematically described as an operation on ***I***:

$$\boldsymbol{I}^{sca} = \boldsymbol{F}\,\boldsymbol{I}^{inc} \qquad (15)$$

where the superscripts refer to scattered and incoming light and ***F*** is the 4-by-4 Müller matrix which contains the information of the scatterer(s). The scattering problem thus reduces to the determination of the elements of ***F***. The scattering of a single particle depends on the ratio between the particle size and wavelength of the light, the shape, orientation and refractive index of the particle. For particles with symmetries or ensembles of scattering particles several matrix elements may vanish or become related to each other (Mishchenko et al. 2002).

2.4.4 Computational methods

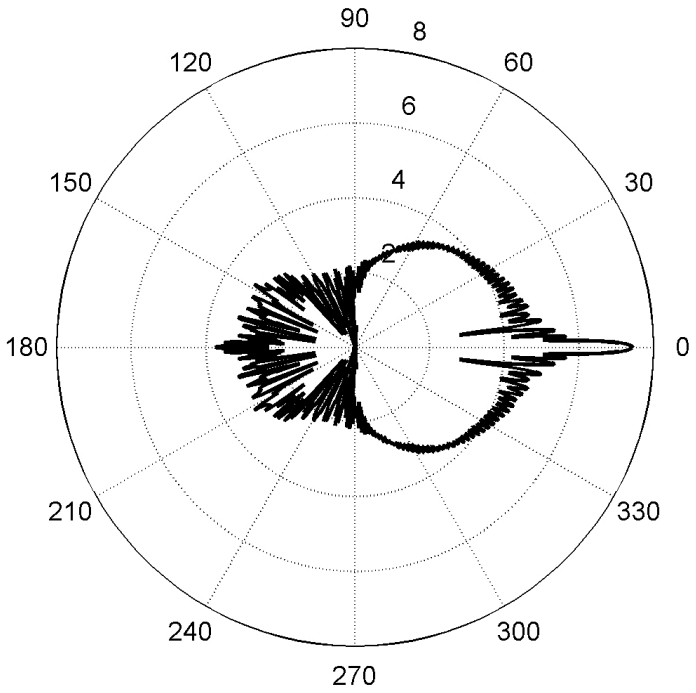

***Figure** 7. Mie scattering pattern of a sphere with refractive index 1.33+0i and size parameter (=circumference of droplet divided by the wavelength of the light) 100. The intensity is on logarithmic scale and 0° and 180° are the forward and backward directions respectively.*

For spherical particles illuminated by a plane monochromatic wave, the scattering can be calculated using series of spherical Bessel functions (Arfken and Weber, 1995). This is the so-called Mie scattering (Bohren and Huffman, 1998), which provides a robust and simple method for light scattering calculations. I wrote a Mie scattering code in Matlab based on the algorithm presented in the book by Bohren and Huffman (1998). The output from the program was tested against other programs and showed to be correct. In figure 7, a Mie scattering pattern from a droplet which is illuminated from the left (180°). Most of the light passes through the droplet, but significant fractions are scattered backwards or the sides. For larger particles, a scattering maximum appears at about 140°, which is the maximum which causes rainbows. The free software MiePlot (available at http://www.philiplaven.com/mieplot.com) is recommended for those who want to learn the basics of light scattering by spherical particles. For non-spherical particles, there are several approaches. The T-matrix method (Mishchenko, 1998) has proven to be useful for particles with an axis of rotational symmetry. However, the size and asymmetry ranges are limited due to numerical caveats. For visible light, the upper limit of particle sizes is a few microns depending on the degree of asymmetry. For larger particles, geometrical optics approximations are valid and ray tracing techniques can be used (Hess et al., 1998). There is, unfortunately, a gap between these methods. For visible light this gap stretches from about 5 to 100 μm. Many particles in the atmosphere are in this size range where light scattering calculations are very tedious.

2.5 Levitation techniques

In order to study freezing processes in droplets, several techniques have been proven useful. Among them *levitation* methods have the great advantage of contactless trapping of a single droplet/particle for an in principle arbitrary time period. Brandt (1989) reviewed several of the techniques, which have their unique characteristics and ranges of usefulness. These techniques include:

- Aerodynamical (http://youtube.com/watch?v=g1rXZXTbRVc)
- Acoustic/ultrasonic (http://www.youtube.com/watch?v=S4exO4CuoSU)
- Optical (http://fy.chalmers.se/f3a/tweezers/movie.html)
- Magnetic (http://www.youtube.com/watch?v=s0MaqQzdutQ)
- Diamagnetic (http://www.youtube.com/watch?v=m-Al7GAnH8Q)
- Radio-frequency
- Superconducting (http://www.youtube.com/watch?v=nWTSzBWEsms)
- Electrodynamical

2.5.1 Electrodynamic balance

Electrodynamic levitation is a robust and useful technique to trap charged particles/droplets with sizes ranging roughly from 1 to 500 μm. The equation of motion of a particle with charge q exposed to an external time- and space-dependent electric field $\boldsymbol{E}(\boldsymbol{r},t)$ in a viscous medium is (Hartung and Avedisian, 1992):

$$m\ddot{\boldsymbol{r}} = q\,\boldsymbol{E}(\boldsymbol{r},t) - mg\,\boldsymbol{e}_z - K_D\dot{\boldsymbol{r}} \qquad (16)$$

where m is the particle mass, $\boldsymbol{r}$ is its position vector, g *is* the acceleration due to gravity, $\boldsymbol{e}_z$ is the unit vector in the vertical z-direction and K_D is the drag coefficient. Dots represent time-derivatives. The

electric field in an EDB is provided by electrodes, usually with a cylindrical symmetry in the z-direction and also mirror symmetric in an xy-plane. These symmetries provide a natural origin of the coordinate system. The electric field is provided by superposition of DC and harmonic AC voltages applied to the electrodes. Hence, the electric field becomes:

$$\boldsymbol{E}(\boldsymbol{r},t)=\boldsymbol{E}_{\boldsymbol{DC}}(\boldsymbol{r})+\boldsymbol{E}_{\boldsymbol{AC}}(\boldsymbol{r},t)=V_{DC}\boldsymbol{e}_{\boldsymbol{DC}}(\boldsymbol{r})+V_{AC}\sin(\omega t)\boldsymbol{e}_{\boldsymbol{AC}}(\boldsymbol{r}) \quad (17)$$

where V_{DC} and V_{AC} are the applied voltages, $\boldsymbol{e}_{DC}(\mathbf{r})$ and $\boldsymbol{e}_{AC}(\boldsymbol{r})$ are the AC and DC electric fields per applied Volt and ω is the angular frequency of the AC voltage. The combination of electrodes of an EDB is required to make the AC field non-constant and even in the z-direction ($\boldsymbol{e}_{AC}(z) = \boldsymbol{e}_{AC}(-z)$). It is important to understand that a plausible AC field is sufficient to trap a droplet and balance gravity. The role of the DC voltage is to lift the droplet to the centre and decrease the droplet oscillation.When a droplet is at some distance from the centre, the AC voltage will cause the droplet to oscillate. The electric field is not constant and the upward force on the droplet when it is in a low position is larger than the downward force when the droplet is closer to the centre. Hence, there will be a net force towards the centre when averaging over time. There are several ways of arranging the electrodes, as shown in figure 8, which all have their pros and cons. There are of course several aspects to consider, such as trapping efficiency, stability issues, electronics and how open the set-up is for observation. The most commonly used arrangements are the hyperboloidal ((a) in figure 8) and the double-ring ((d) in figure 8). The hyperboloidal has a good trapping efficiency, i.e. it can trap particles with low charge without having to apply large AC voltages. The double-ring EDB has the great advantage of an open geometry; the trapped particle is observable from above, below and 360º in the horizontal plane. On disadvantage is that the rings must be held in place and charged by rods, which disturbs the fields to some extent.

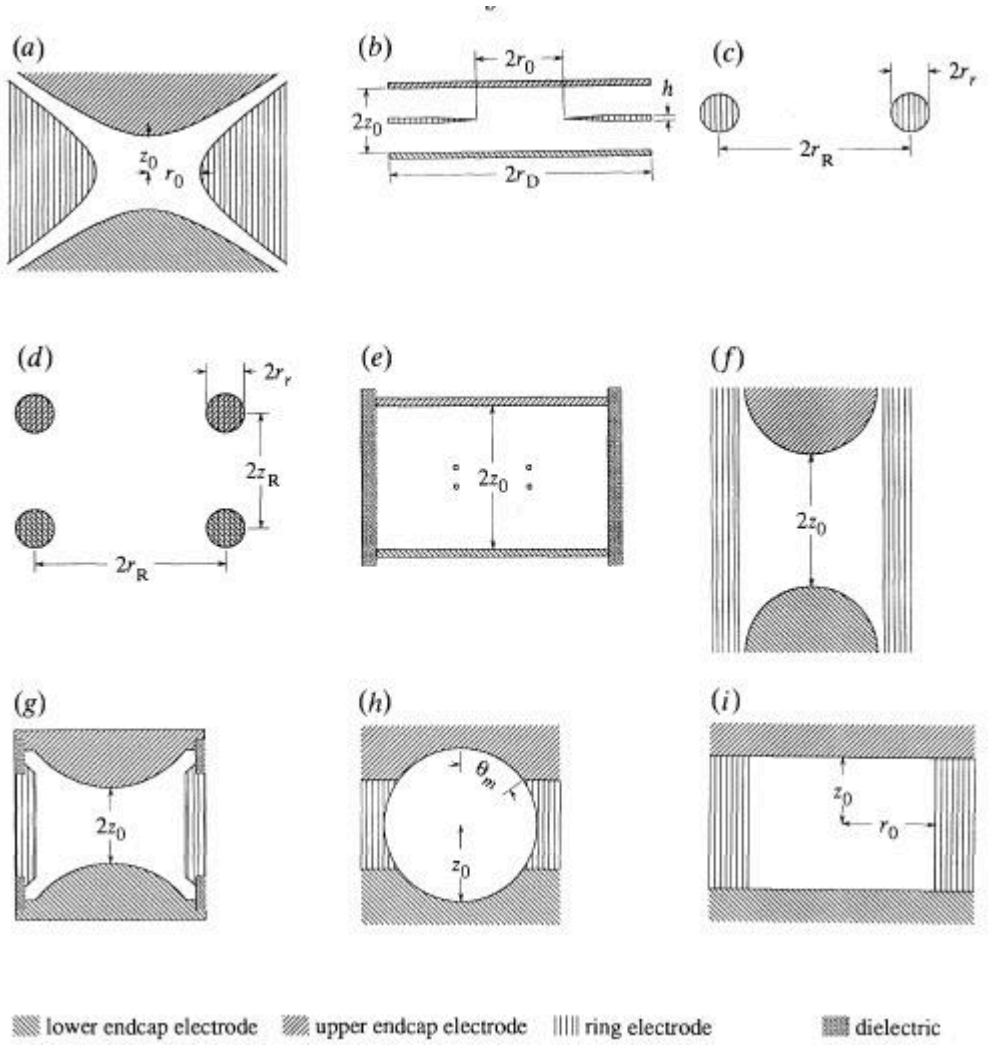

Figure 8. *Sectional view of some possible electrode configurations for an electrodynamic balance. All shapes are axisymmetric. (a) Ideal hyperboloidal electrodes (surfaces extend to infinity). (b) One form of the 'triple-disc' configuration. (c) Single-ring configuration . This shape does not incorporate electrodes for balancing gravity, so it can only suspend particles in dynamic equilibrium. (d) Double-ring configuration. (e) Double-ring/double-disc configuration. (f) Spherical endcap electrodes and a cylindrical ring electrode. (g) Bihemispherical configuration. (h) Spherical void (SVEL) configuration. (i) 'Pillbox' configuration. Figure is reproduced from Hartung and Avedisian, 1992 with permission from The Royal Society of London.*

3. Experimental techniques

In this chapter I will describe the experimental techniques used in the studies which the papers are based on. Section 3.1 describes an EDB set-up which I developed and papers I-III present studies performed using this set-up. In section 3.2 the bistatic lidar technique, which was used in paper IV, is described. The vacuum system used for the molecular beam studies presented in paper V is described in section 3.3.

3.1 Electrodynamic balance set-up

In order to study the freezing of single micrometer sized droplets, a levitation set-up based on the EDB principle was developed. A schematic view of the set-up is shown in figure 9 and a picture is shown in figure 10.

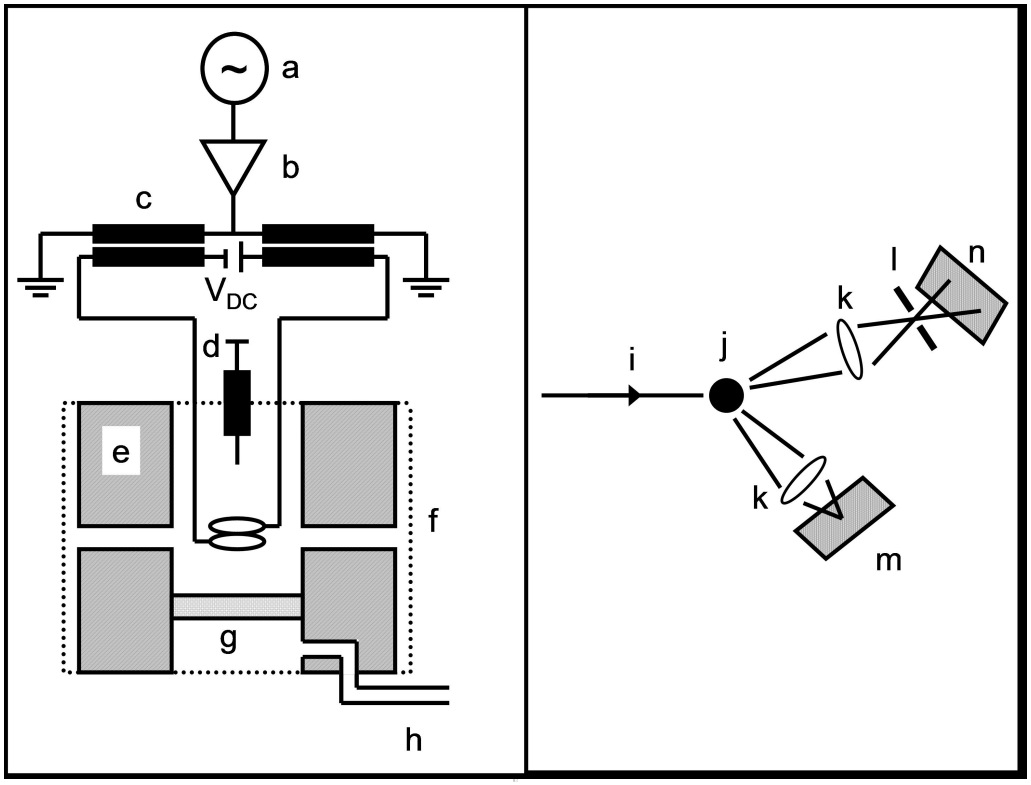

***Figure 9**. Schematic view of the EDB set-up used for droplet levitation experiments. Left panel: a) signal generator, b) amplifier box, c) transformers, d) syringe, e) copper blocks, f) quartz cylinder, g) sintered plate, h) gas inlet. Right panel: optical system as seen from above. i) incoming laser beam, j) trapped droplet, k) convex lenses, l) aperture, m) CCD plate used to record regular movies, n) CCD plate used to record light scattering patterns.*

The idea is to have a double-ring electrodynamic trap in a temperature regulated environment with an open geometry. Two concentrical cylindrical shells of copper with a 360° observation slit are surrounded by a quartz shell. The copper blocks are cooled by running cooled air through them and temperature controlled by electric heating circuits. The temperature is measured by Pt-100 sensors

inserted into holes in the blocks. It can be useful to sometimes have a smooth flow through the chamber, which is obtained by having a sintered plate in the lower part of the chamber. Laboratory gas is thermalized in a special circuit in the lower copper block and is subsequently released below the sintered plate.

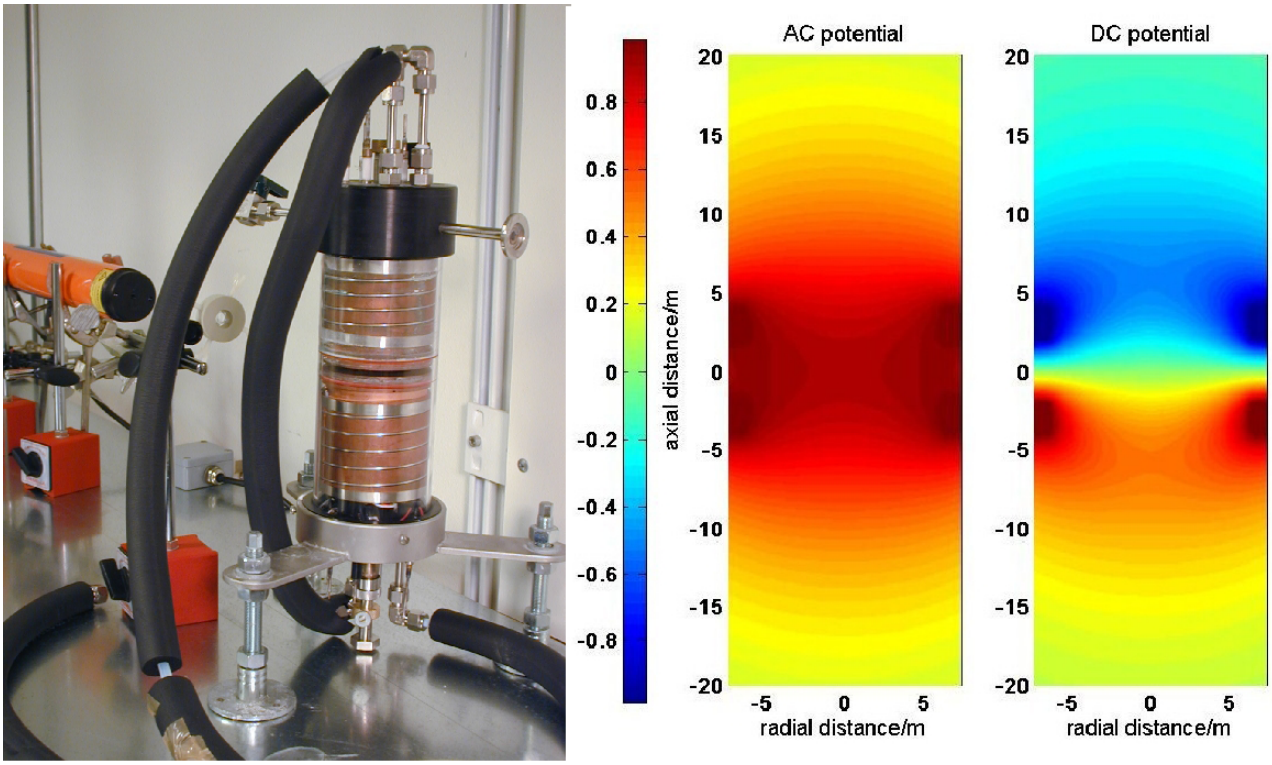

***Figure 10**. Left panel: Picture of the levitation set-up. Right panel: The electric potentials per applied volt for the AC and DC potentials respectively.*

In order to obtain levitation and trapping of the droplets, we applied a superposition of AC and DC voltages provided by a home-built voltage amplifying system. The voltage from a signal generator was current amplified and an array of low-effect transformers amplifies the AC voltage to maximum 1500 V_{rms} @ 100 Hz. The DC voltage applied was generally less than 50 V. The rings are located 4 mm away from each other and their inner radius is 6.5 mm. We could solve the Laplace equation $\nabla^2 \phi = 0$ for the electric potential numerically. The potentials from the AC and DC field are shown in figure 10.

In order to understand the way different droplets move in the electrodynamic trap, I made a Matlab model solving the equations of motion for a charged droplet in the EDB. Two typical droplet trajectories are shown in figure 11. This shows that droplets can be trapped without having a DC voltage applied. It also shows that the phase of the AC voltage generally has no effect on the long-term movement of the particle. Numerous model runs were performed to obtain a picture of which droplet characteristics were suitable for the trap. Since the droplets enter the trap from above, this situation was modelled. If the droplets were too small (typically less than 5 μm in diameter) they could not enter the area between the rings, but instead moved to the side. Large droplets (larger than 200 μm) either fell right through the trap or, if a very high AC voltage was applied, were unstable in the trap. The behavior of the modelled droplets corresponds well to the real situation.

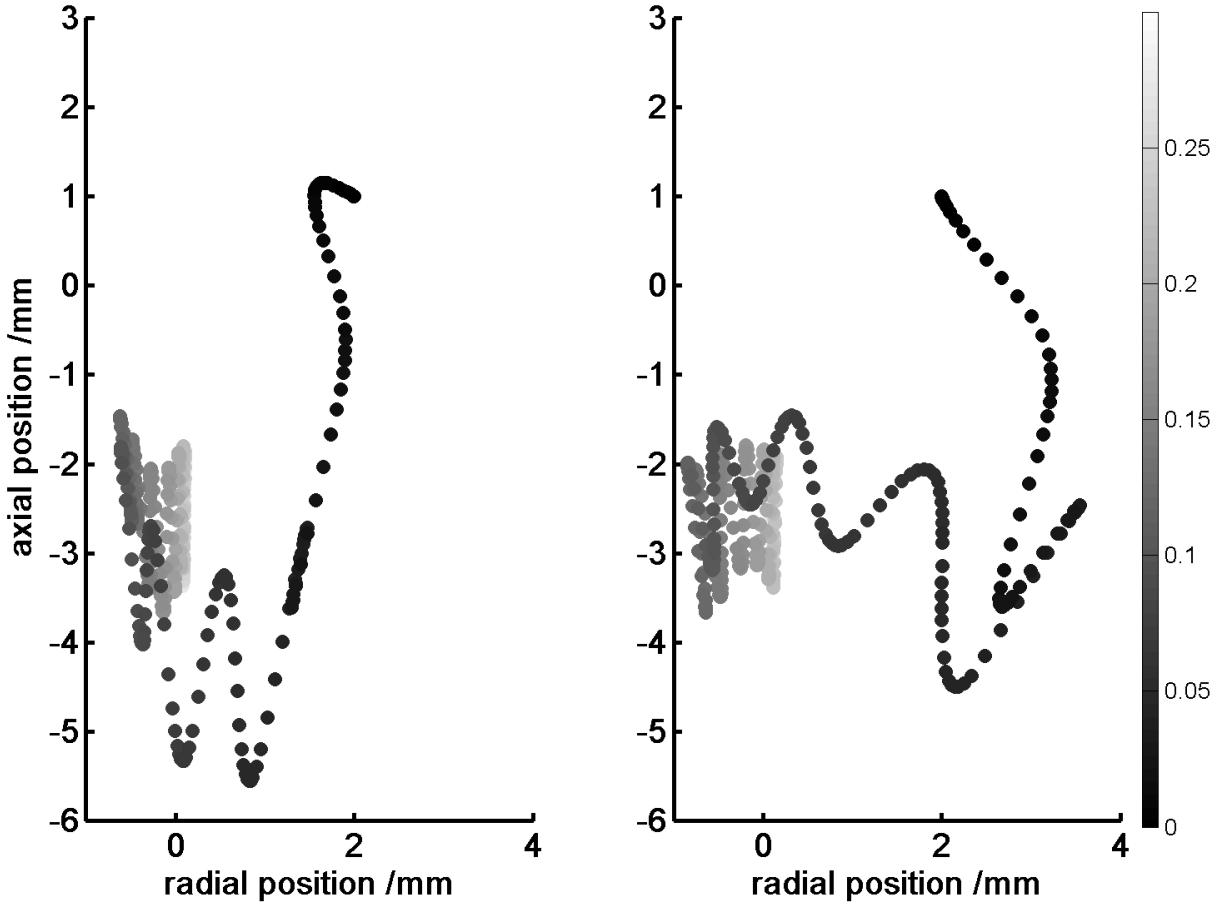

Figure 11. *Modelled droplet trajectories in the EDB. Identical water droplets were released in rest 2 mm on the side and 1 mm above the centre. They had a diameter 100 μm and $6*10^6$ elementary charges each. No DC voltage is applied. The AC voltage amplitude was 1500 V @ 50 Hz. The difference between the two plots are that the AC voltage was phase shifted π/2 in the right panel. The time in seconds is shown in the gray scale.*

Information about the trapped droplets is obtained from two cameras, one which records the ”ordinary” movie of the droplet and one which records the light scattering pattern, which for spherical particles typically looks like the one shown in figure 9. Since the illuminating laser light is linearly polarized perpendicular to the scattering plane, the scattered light from a spherical particle is also completely linearly polarized. Hence, any deviations from sphericity can be detected by placing a polarization filter in front of any of the cameras. The size of droplets can be determined from the scattering pattern by comparing with predictions from Mie theory. In our set-up the size determination is done by counting the fringes and compare with a computationally derived first degree polynomial to compute the size.

3.2 Bistatic lidar set-up

Cirrus clouds are high and optically thin clouds which cover about 20% of the Earth (Liou, 1986). Due to their altitude, cirrus clouds are considered to have a net heating effect on the atmosphere (Liou, 2002). A measurement approach to examine the properties of cirrus clouds is Lidar (LIght Detection And Ranging). It is based on the same principle as the radar, using visible light instead of radio waves. Short intense pulses of laser light are sent from the ground up into the atmosphere and the scattering is recorded with time resolution at some location, often at the same place as the laser, hence observing the backscattering. Due to the time resolution of the data, height resolved information on the scatterers in the atmosphere can be retrieved. It is, however, possible to have the observation unit at another location, and observe the scattering at a non-backscattering angle. Such a set-up, a *bistatic lidar*, which is shown in figure 12 was used at ALOMAR (Arctic Lidar Observatory for Middle atmosphere Research) outside Andenes (69° N, 16° E) in northern Norway.

The laser, located at the main ALOMAR observatory, was a pulsed Nd:YAG laser operating at 532 nm. The measurement station was located 2.1 km away from the laser. The measurements were trigged using an extra telescope directed to the lower portion of the beam. The main telescope recorded light at angles between 130° and 170°, corresponding to altitudes between 1.5 and 11 km. In front of the receiver were a rotatable half-wave plate and a linear polarizer. Using this arrangement, the degree of linear polarization, $P_L = \sqrt{Q^2 + U^2}/I$ could be calculated.

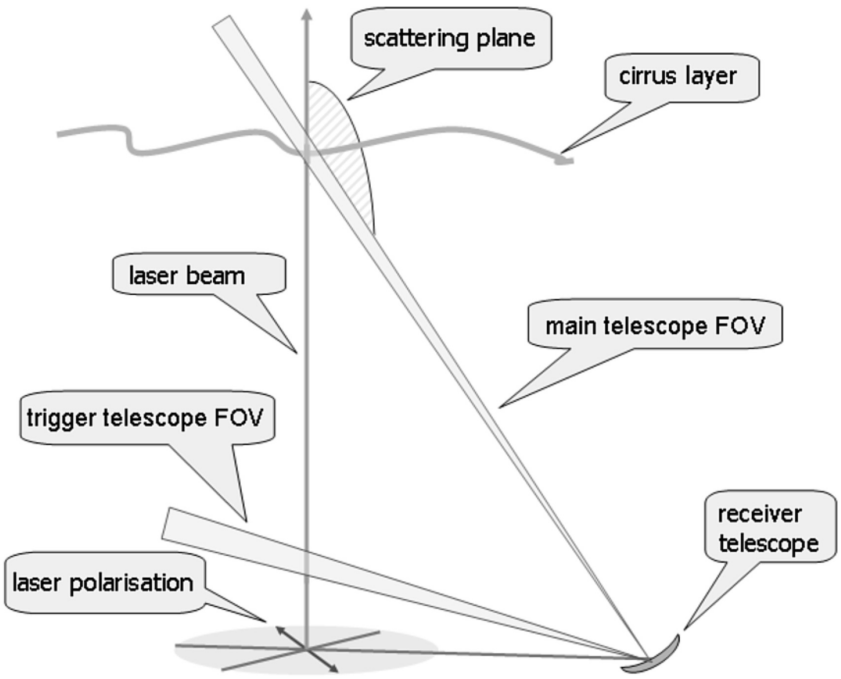

***Figure 12**. Schematic view of the bistatic lidar set-up. The laser polarization is directed 23.8° away from the scattering plane.*

3.3 Molecular beam set-up

In the molecular beam studies presented in paper V, we used the ultra-high vacuum equipment described in detail by Andersson et al, 2000. A molecular beam was generated by a pulsed source and let into successive chambers with lower and lower pressure. The principle is shown in figure 13. On its way the molecular beam pulses were chopped by a rotating plate with slits in order to make the pulse as square-shaped as possible. The beam finally entered a chamber with a graphite surface (12-by-12 mm) directed in a 45° angle from the beam. In this chamber the pressure was typically $2*10^{-9}$ mbar. The molecular scattering was observed by a rotatable quadrupole mass spectrometer. Additionally, a laser beam was utilized to probe ice layer formation on the surface.

In the present experiments, the molecular beam was composed of helium and N_2O_5.and a minor HNO_3 component. The partial pressure of N_2O_5 in the pulsed molecular beam source was controlled by varying the temperature of the N_2O_5 container. During ice nucleation experiments, water vapor was added by a special inlet into the chamber surrounding the graphite surface.

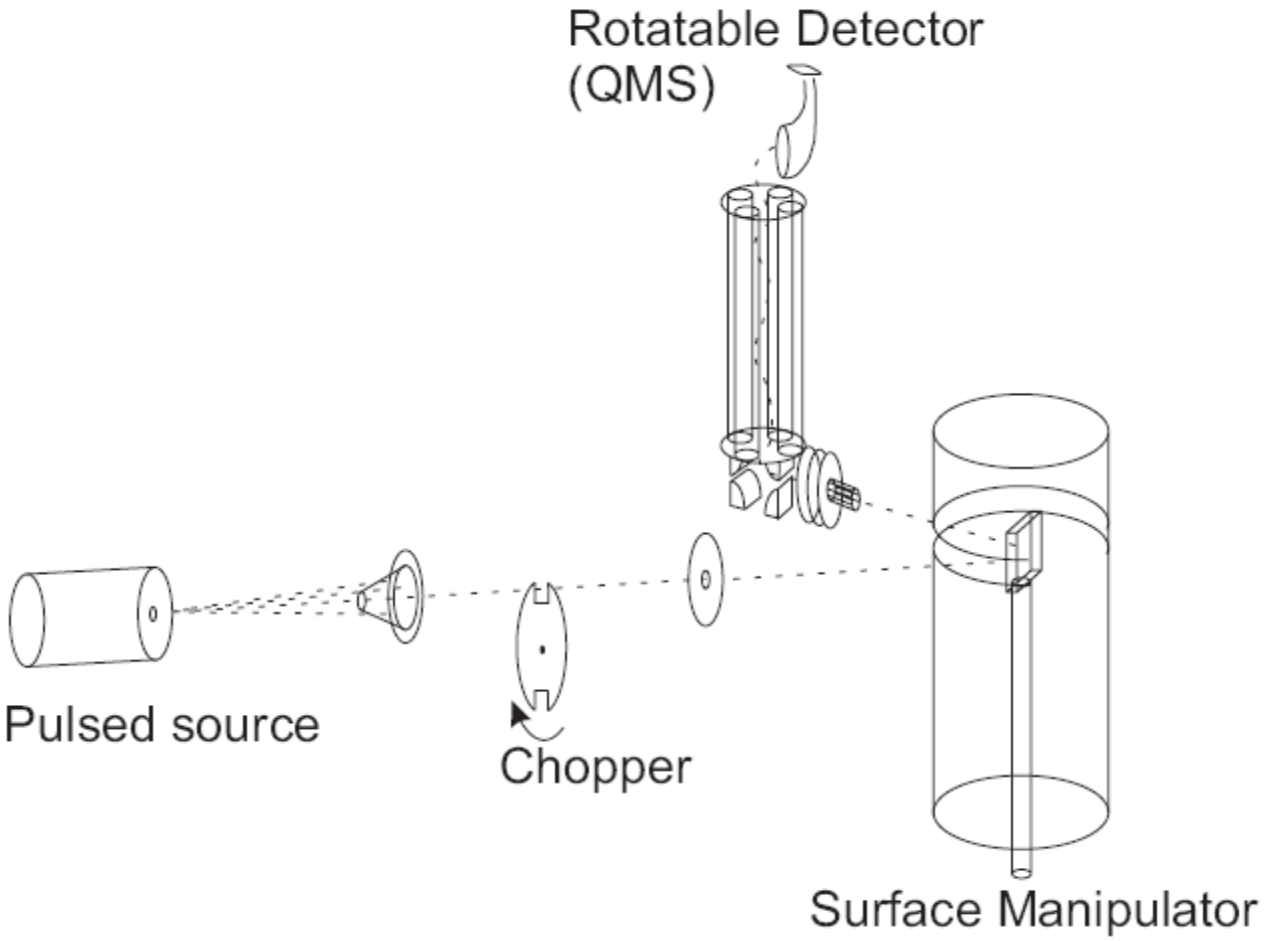

Figure 13*. Schematic view of the molecular beam equipment, used to study gas-surface interactions.*

4. Results and discussion

In this chapter the results from the papers included in the thesis are summarized. Papers I and II concern freezing of evaporating oxalic acid solution droplets. In paper III we present results from freezing experiments with pure water droplets colliding with dispensed kaolinite dust. Experimental results from lidar studies of Arctic aerosol and clouds are presented and compared with computational results in paper IV. Results from studies of the interaction of N_2O_5 with graphite surfaces and of N_2O_5- and HNO_3-mediated ice deposition on graphite are presented in paper V

4.1 Freezing of oxalic acid solution droplets

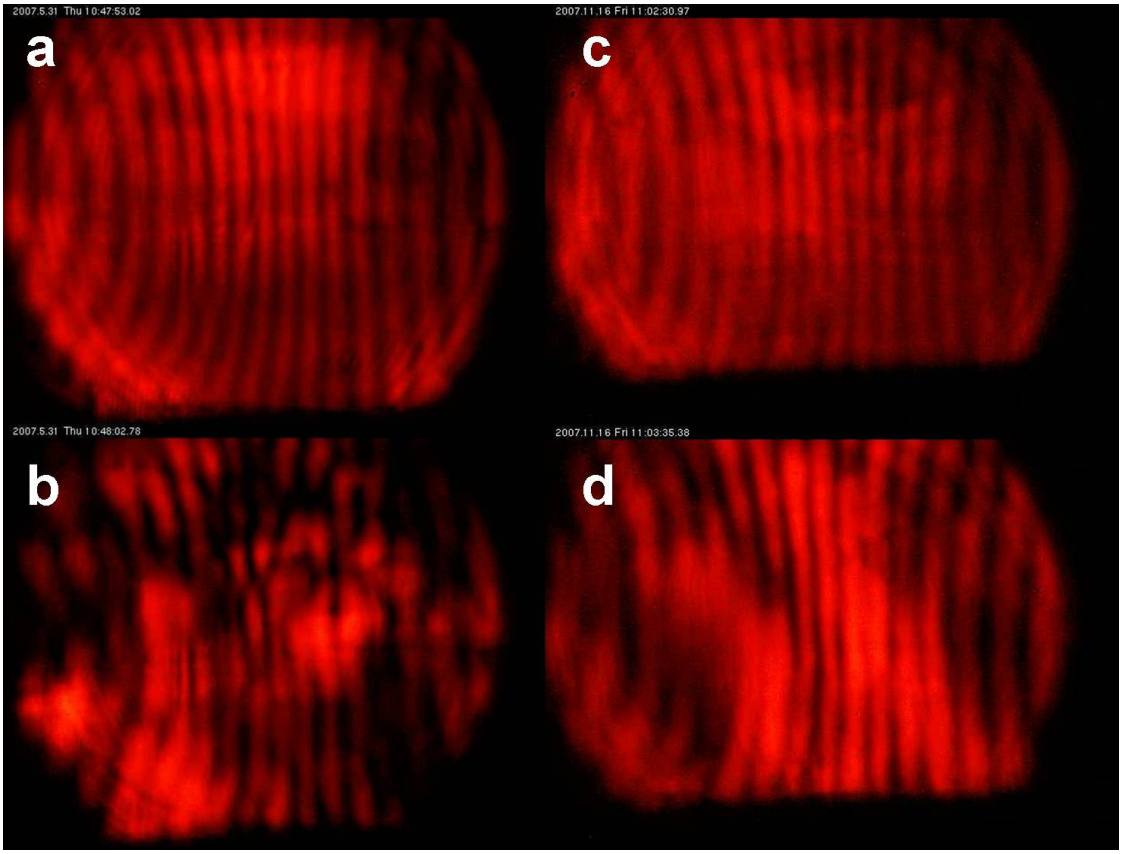

Figure 14. *Light scattering patterns. a) is a liquid oxalic acid solution droplet, which freezes and obtains the scattering pattern shown in b). c) & d) show a pure water ice particle directly and 70 s after freezing, respectively.*

As an initial test of the levitation chamber, we checked whether it could reproduce the homogeneous freezing rates of pure water previously reported in the literature, e.g. Duft and Leisner (2004), and the results showed a good agreement. In paper I, the focus was to show that evaporating oxalic acid (OA) solution droplets freeze heterogeneously at temperatures as high as 248 K. Droplets with an initial concentration of 0.1 M OA were trapped in the EDB at various temperatures. Due to the relatively dry conditions, the droplets evaporated continuously during the periods they were trapped. Droplets

became supersaturated with respect to OA and precipitates were formed inside the droplets. At some moment, a phase transition occurred. Phase transitions were visible in both the "ordinary" movies, as an increase in the brightness of the particle, and in the scattering pattern. The difference in scattering pattern was much more pronounced when OA was present in the droplet than in pure water. This can be seen in figure 14.

By comparing the initial droplet volume and the volume just before the phase transition, the OA concentration could be calculated. Results are presented in figure 15. At the lower temperatures used (236-240 K) some droplets underwent phase transition instantly after injection to the trap while others stayed liquid for a few minutes. At the higher temperatures, no phase transitions occurred directly, but rather after a period of evaporation.

In order to investigate the nature of this phase transition we logged the DC voltage while keeping the droplet in a fixed position. For droplets with a relatively low OA concentration at phase transition, these experiments revealed that the evaporation was slowed down, although still progressing. This is clear evidence of the formation of an ice phase with a lower vapor pressure than the liquid. Analyses of the times before freezing showed that the observed freezing could not be explained by heterogeneous freezing due to pre-existing ice nuclei within the droplets. Hence, we concluded that the freezing could only be explained by heterogeneous freezing caused by OA dihydrate precipitates formed inside the evaporating droplets. At no occasion droplets froze when the OA concentration was lower than the solubility expected from extrapolation of experimental data (Apelblat and Manzurola, 1987). There are clearly differences in our results and the previously reported results on heterogeneous freezing of OA solution droplets in oil emulsion (Zobrist et al, 2006).

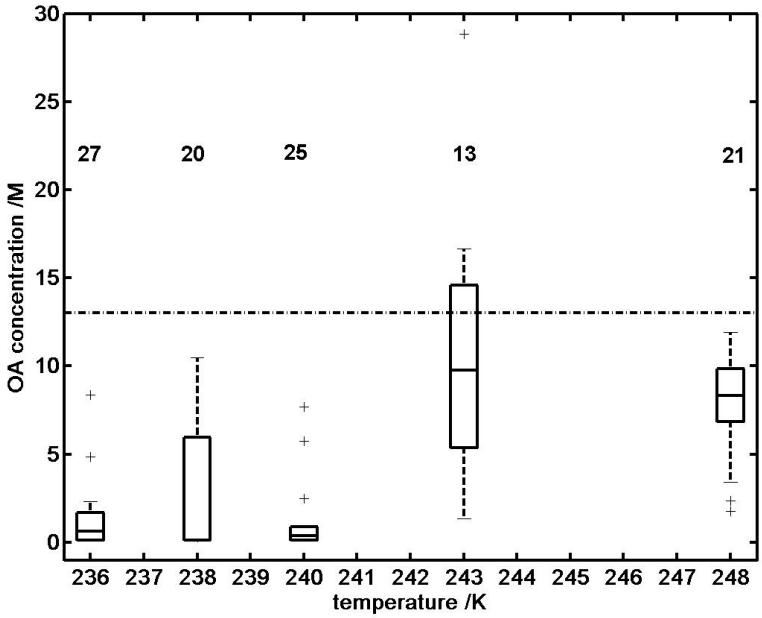

Figure 15. *Boxplot of OA concentrations at the liquid-solid phase transition for different temperatures with the number of droplets indicated for each temperature. The dash-dotted line at 13 M shows the concentration expected in a dry OAD particle. Plus signs represent outliers as defined by MATLAB´s boxplot function. The uncertainty in concentration increases with increasing concentration. No point is above the 13 M-line within uncertainty.*

In the study which is presented in paper II, the temperature was kept constant at 245 K and the initial OA concentration was varied. Four initial concentrations were used (0.032, 0.1, 0.32 and 1 M), related to each other by the square root of 10. About 20 droplet experiments per initial concentration were performed. Phase transitions occurred within a range of estimated concentrations between 0.4 and 17 M. About 50% of the droplets with initial concentration 1 M froze instantly after injection into the EDB. No major differences in the freezing concentrations were found when varying the initial concentrations. A histogram (figure 16) over the phase transition concentrations indicates at least two modes in the distribution of concentrations. To summarize, the two studies show that evaporative freezing may occur at relatively high temperatures for solutions of organic compounds. The effects of evaporation-induced freezing under atmospheric conditions are currently unknown, and should be subject of further studies.

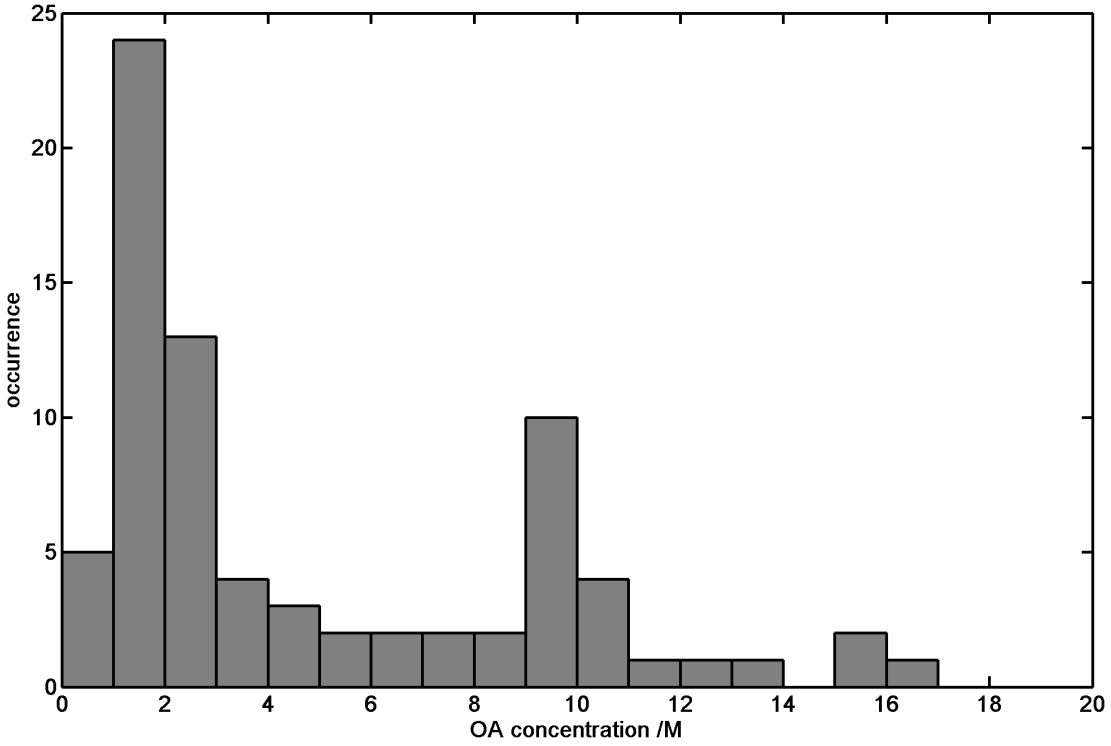

Figure 16*. Histogram of the phase transition concentrations.*

4.2 Contact freezing experiments

In paper III contact freezing experiments with kaolinite particles colliding with pure water droplets are presented. We developed a kaolinite dust dispenser which produced a fairly stable flow of aerosol. This flow was either let out through the laboratory ventilation or directed into a special copper piece in contact with the inner copper walls of the chamber. This thermalized the kaolinite aerosol before entering the chamber right below the position of a trapped droplet. By measuring the particle number concentration between the rings, we obtained a value which was proportional to the number of collisions per unit time experienced by a trapped droplet.

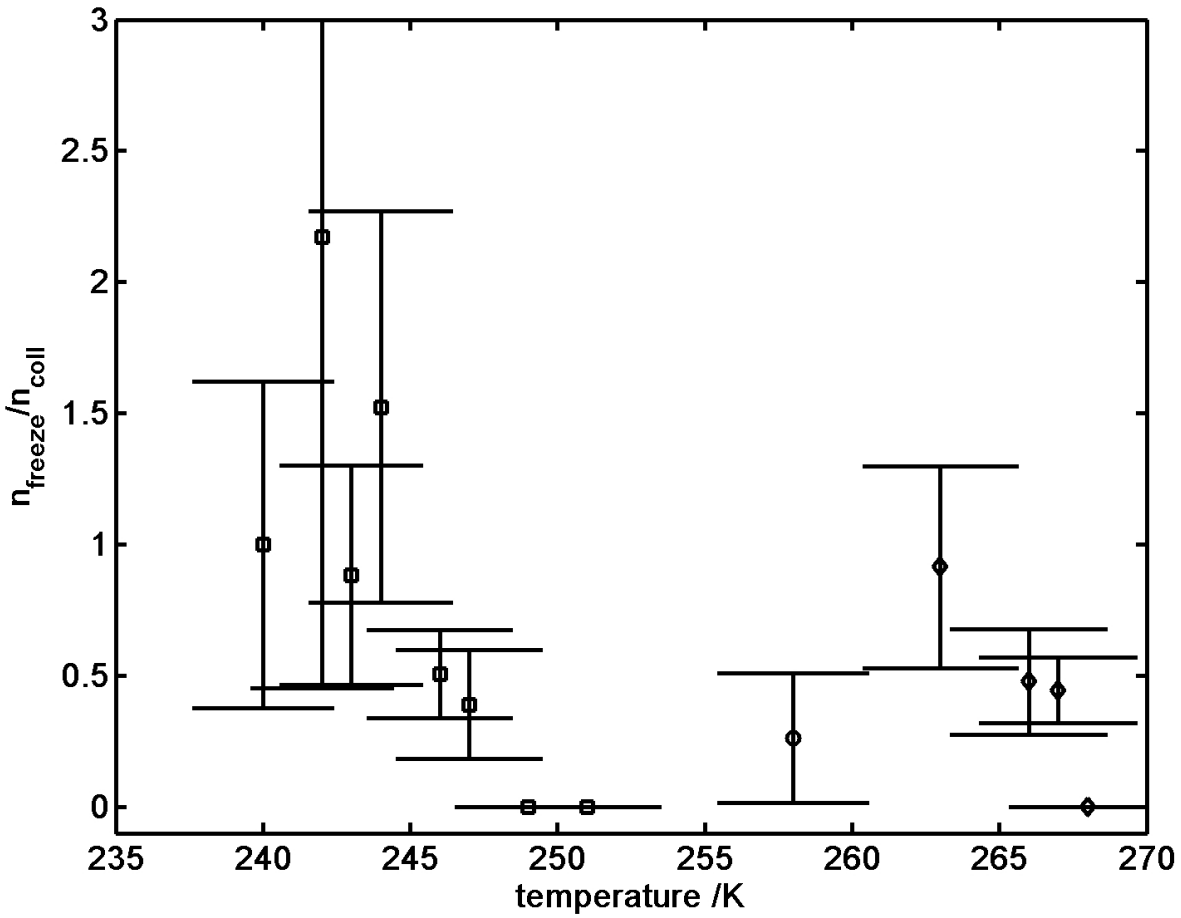

Figure 17*. Estimated number of freezing events per collision. Squares represent experiments at dry conditions, circles intermediate flow of humid air and diamonds high flow of humid air.*

The collisions between the water droplets and the kaolinite induced freezing in a large temperature range. Assuming that at temperatures below 243 K the droplets freeze on the first collision, a proportionality constant between the number of collisions and the particle number concentration could be calculated. Hence, the freezing efficiency, i.e. the number of freezing events per collisions, could be estimated as shown in figure 17. The results indicate that one ore a few collisions are usually sufficient to induce freezing under the conditions used in this study. The freezing probability has been found to increase with increasing relative humidity. The mechanism behind this behavior is interesting from a fundamental point of view since the conditions were neither cold, nor humid enough for deposition ice nucleation on the kaolinite particles before contact with the liquid droplets (Salam et al. 2006).

4.3 Bistatic lidar experiments and light scattering calculations

During the CABLE (Cooperative ALOMAR Bistatic Lidar Experiment) campaign the degree of polarization, P_L, in Arctic aerosol and clouds was measured in Northern Norway. The full results from experiments and light scattering calculations are presented in paper IV. During cloud free conditions,

the light scattered by aerosol particles had degrees of linear polarization, between 0.6 and 0.7. Light scattering calculations showed that, in general, spherical particles with common types of size distributions and refractive indices (Omar et al., 2004) were unable to cause P_L values that low. Particles with non-spherical shapes had to be introduced to explain the observed depolarization produced by aerosol particles at relatively low altitudes. When thin and mildly opaque cirrus clouds were present P_L values were between 0.2 and 0.4. We used T-matrix calculations to investigate the scattering from cylinders and the results, which are shown in figure 18, indicate that at 7.8 km altitude, the minimum in P_L values possible from these types of particles is about 0.2 for a scattering angle of 165°.

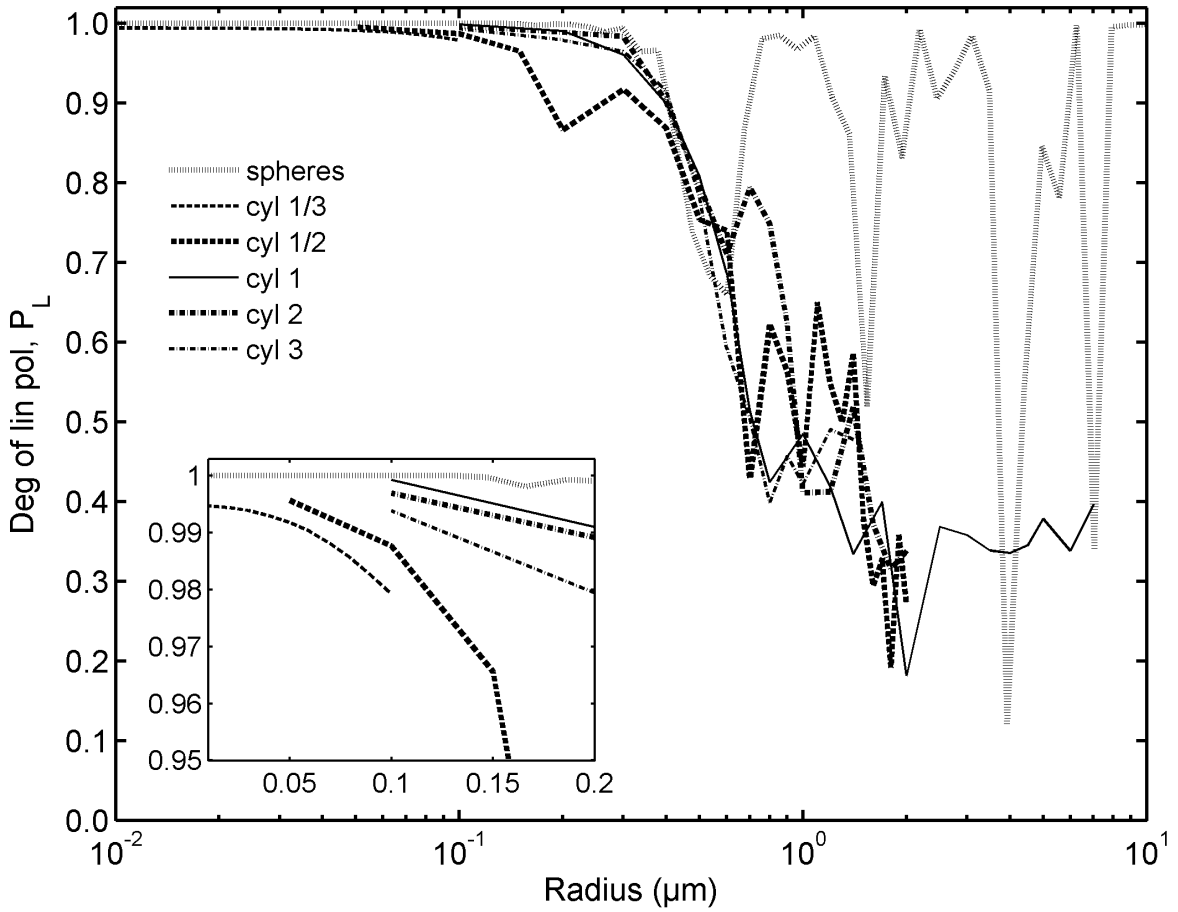

Figure 18. *P_L values at an scattering angle of 165° (corresponding to 7.8 km altitude) as functions of radius for randomly oriented cylindrical particles with different aspect ratios. The particles are assumed to consist of ice and to be monodisperse. Results for monodisperse spheres are included for comparison.*

Aerosols often have log-normal size distributions (Hinds, 1999). We calculated the degree of polarization for log-normally distributed aerosol and randomly oriented particles over the whole angular range 130-170°. Cylinders and spheroids with a mean radius of 1 μm and various aspect ratios all had P_L values varying between roughly 0.3 and 0.5.

We also investigate light scattering from larger ice particles using the COPE database (Hess et al., 1998), see figure 19. In these calculations surface roughness was modelled as a random tilt angle of the surface of the particles. The maximum tilt angle was used as a measure of the roughness. In figure 19 the experimental results are compared with the results from calculations. The ray-tracing calculations were concluded to reproduce the experimental results if a suitable degree of surface roughness was introduced. This does not conclusively show that the ice particles were indeed hexagonal ice columns, since other shapes may produce similar results. Particle orientation effects may also have influenced the experimental results. To conclude, the study illustrates that the bistatic lidar method may provide a useful technique in the development of an improved cirrus cloud climatology and to help validate other techniques being used.

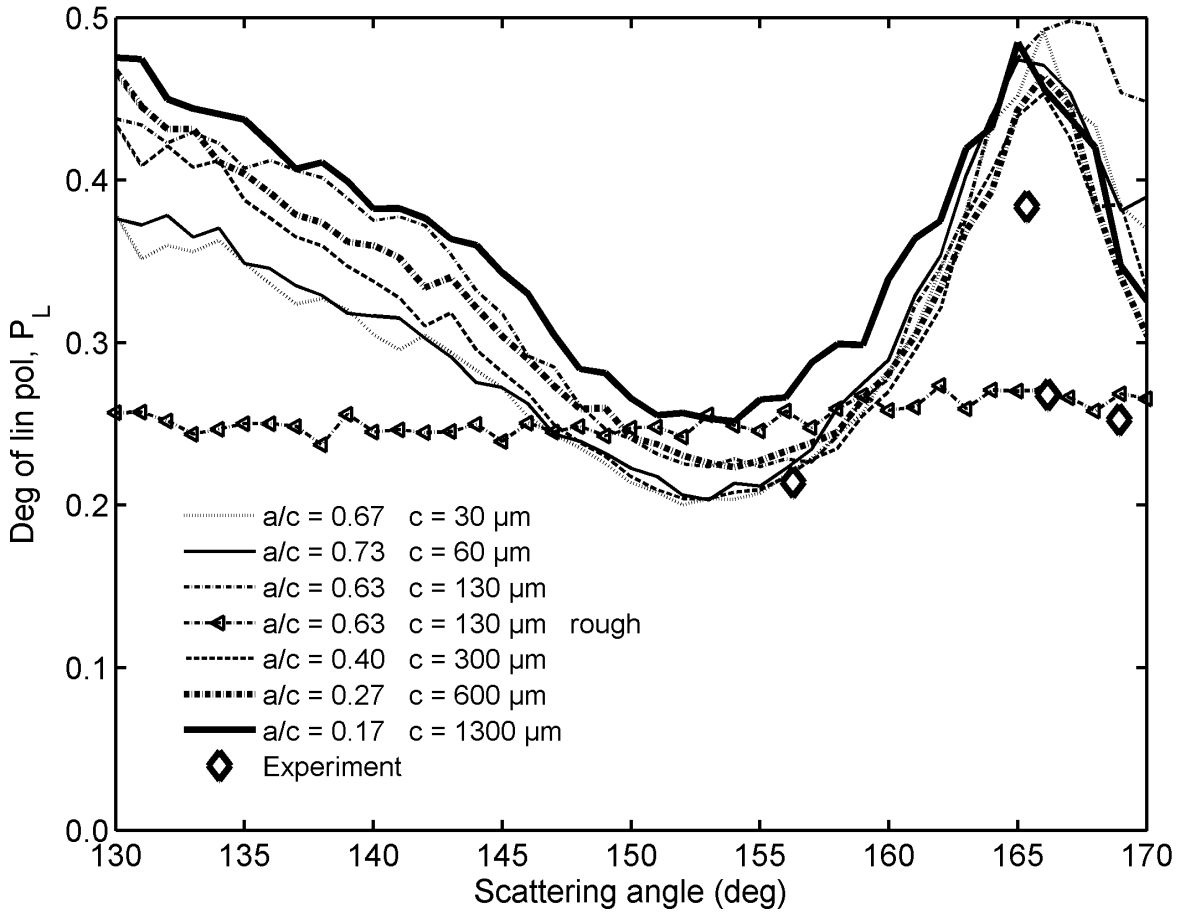

Figure 19. *Degree of linear polarization from measurements on cirrus clouds (diamonds) and calculated with a geometric optics ray-tracing method for randomly oriented hexagonal columns with different dimensions (lines). One data set (marked "rough") simulates extensive surface roughness of the particles.*

4.4 Interactions between nitrogen pentoxide, nitric acid, graphite and ice

In paper V the formation of adsorbed layers of dinitrogen pentoxide, nitric acid and water on graphite was studied by molecular beam and light scattering techniques. The overall aim was to contribute to the

fundamental understanding of ice film formation on solid surfaces. Of special interest was the influence of co-adsorption of different components on deposition freezing. The graphite surface may be looked at as a very simplified model of soot particles in the atmosphere. Molecular beam techniques were initially used to study the desorption kinetics of the N_2O_5/graphite system. The desorption kinetics of N_2O_5 on graphite were well described by the Arrhenius equation, and an activation energy of 0.24 ± 0.03 eV and a pre-exponential factor of $2.3 \cdot 10^{(10 \pm 0.73)}$ s^{-1} were determined from the experimental data. The N_2O_5 binding energy was concluded to be stronger than the H_2O-graphite binding energy, which is of potential importance during co-deposition of the two gases.

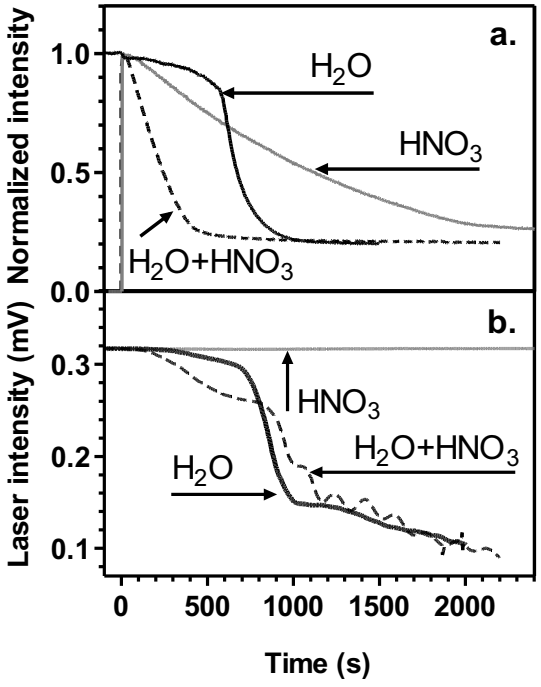

***Figure 20**. Co-deposition of H2O and HNO3 on graphite at 170 K: a) Normalized helium scattering intensity as a function of time during build-up of H2O, HNO3, and mixed H2O-HNO3 adlayers on graphite. The molecular beam and the water vapor pressure were turned on at time zero. b) Light scattering intensity measured simultaneously for the three cases in a).*

Elastic helium scattering and light scattering were used to follow the formation of pure and mixed ice layers on the surface. Helium scattering made it possible to follow how the bare surface became covered with an adlayer over time. Light scattering made it possible to identify occasions when the ice films grew to sufficient thickness to produce constructive and destructive interference of the scattered light. Typical results at a surface temperature of 170 K are illustrated in figure 20. Adsorption of N_2O_5 and HNO_3 resulted in formation of thin adlayers under the conditions employed in the study. In co-adsorption experiments, N_2O_5 was concluded to facilitate the formation of thick N_2O_5-H_2O ice layers at 155 K. In the same way co-adsorption of HNO_3 and H_2O resulted in the formation of thick layers at 170 K. The adlayer formation kinetics were substantially different compared to formation of pure water ice

films. Further studies should examine the mechanisms by which HNO_3 and similar components act to decrease the partial pressure of water required for deposition freezing to occur under atmospheric conditions.

5. Outlook

The freezing of evaporating oxalic acid solution droplets is potentially important result, but there are several questions that should be addressed in further research. Within the ranges of temperatures and initial concentrations used in the two studies (papers I & II) freezing appears to be a general phenomenon. Is this a unique property of OA or do a large number of substances have the same effect? In earlier in-situ wave-cloud studies by Cotton and Field (2002), droplets freezing was observed during evaporation. Could formation of precipitates that act as heterogeneous ice nuclei be a part of the explanation for these observations?

We also need to know the exact mechanism of the phase transition observed in OA solution droplets. Droplets become both supersaturated and supercooled in the trap. Does the OA precipitate form long before the freezing or do crystallization and freezing happen almost simultaneously? Where does the freezing start, at the surface or in the bulk? In order to investigate these issues, I think continued work with an improved EDB set-up could provide further insights. Improvements could include using fast cameras, microscopic lenses and spectroscopic methods. It would also be interesting to see if there is a lower size limit which prevents freezing of smaller (<1 μm) droplets. Here, cloud chamber or flow tube studies may prove useful.

The collision freezing study vindicated the previous study by Pitter and Pruppacher (1973) at the higher relative humidities of our study. The dependence on relative humidity is interesting from a fundamental point of view. Why would water vapor in the surrounding air enhance the contact freezing efficiency of kaolinite dust? Since the relative humidity is below water saturation, ice is not expected to deposit on the kaolinite particles (Salam et al, 2006). In the study by Salam et al. (2006), they observed the growth of kaolinite particles to detect deposition of ice. Could small ice crystals form in cavities of the kaolinite particles? Spectroscopic detection of minor amounts of ice or microscope are techniques which may help to solve this question. There are also several additional questions concerning contact ice nucleation which needs to be addressed. What effect does the impact velocity have? What is the influence of the sizes of the droplets and particles?

The scientific understanding of homogeneous freezing is fairly good. Koop et al. (2000) provided a reasonably consistent theory to determine the homogeneous freezing efficiencies of aqueous solutions. The discussion of bulk versus surface nucleation may have temorarily stopped due to the article by Sigurbjörnsson and Signorell (2008). They show that the arguments for surface nucleation are based on erroneous assumptions in the data analysis, and new detailed experimental studies will be required to further address the issue. Heterogeneous freezing, on the other hand, has no unifying theory to explain the observations. The cause is of course the complexity of the issue; there are too many parameters to deal with. There are many hours of tedious lab work left to be done.

The bistatic lidar technique has proven to be a useful tool in the investigations of aerosols and clouds. Combined with an ordinary backscatter lidar, the amount of information which can be extracted is large. The technique can be further improved by measuring the Stokes parameters Q and U individually.

One major future challenge is to improve the computational techniques for light scattering of non-spherical particles. The T-matrix method, although very useful for smaller particles, has intrinsic

limitations in size range. There is, to my knowledge, no computationally feasible technique which works for general non-spherical particles at sizes around 10 μm.

The properties and action of clouds in the upper troposphere and lower stratosphere are of central importance to our understanding and prediction of climate change. A molecular level understanding of key processes will help to better describe the formation and development of cloud particles, and one important example is the uptake of water on aerosol and ice particles. The molecular beam experiments described in this thesis provide a starting point, and further research should aim at higher temperatures and systems of increased complexity.

6. Acknowledgements

Jag vill tacka

Min handledare Jan Pettersson för all hjälp och uppmuntran under dessa år.

Alla andra jag har samarbetat med under den här tiden: Christophe, Frans, Georg, Matthew, Mattias, Liza, Patrik, Philipp och Shahriar.

Benny och Thomas för hjälp med de världsliga tingen som är så nödvändiga när man ska gör experiment.

Alla andra på Atmosfärsvetenskap.

Släkt och vänner.

Och, sist men verkligen inte minst, min familj, som fördubblades i antal under den här tiden.

7. References

Andersson, P. U., Någård, M. B., Bolton, K., Svanberg, M. and Pettersson J. B. C., "Dynamics of Argon Collisions with Water Ice: Molecular Beam Experiments and Molecular Dynamics Simulations", *Journal of Physical Chemistry A*, 104, 2681-2688, **2000**.

Apelblat, A., and Manzurola,E., "Solubility of oxalic, malonic, succinic, adipic, maleic, malic, citric, and tartaric, acids in water from 278.15 to 338.15 K", *Journal of Chemical Thermodynamics*, 19, 317-320, **1987**.

Arfken, G. B. and Weber, H. J., "Mathematical methods for physicists", Academic Press, San Diego, **1995**.

Arrhenius, S. "On the Influence of Carbonic Acid in the Air upon the Temperature of the Ground", *Philosophical Magazine and Journal of Science*, Series 5, 41, 237-276, **1896**.

von Blohn, N., Mitra, S. K., Diehl, K. and Borrmann, S., "The ice nucleating ability of pollen Part III: New laboratory studies in immersion and contact freezing modes including more pollen types", *Atmospheric Research*, 78, 182-189, **2005**.

Bohren, C. F. and Huffman, D.R., Absorption and Scattering of Light by Small Particles, John Wiley & Sons, Inc., New York, **1998**.

Brandt, E. H., "Levitation in Physics", *Science*, 243, 349-355, **1989**.

Cantrell, W. and Heymsfield A., "Production of ice in tropospheric clouds: A review", *Bulletin of the American Meteorological Society*, 86 , 795-807, DOI:10.1175/BAMS-86-6-795, **2005**.

Davis, E. J., Buehler, M. F. and Ward, T. L. "The double-ring electrodynamic balance for microparticle characterization", *Review of Scientific Instrument*, 61, 1281-1288, **1990**.

Djikaev, Y. S., Tabazadeh, A., Hamill, P. and Reiss, H., "Thermodynamic Conditions for The Surface-Stimulated Crystallization of Atmospheric Droplets", *Journal of Physical Chemistry*, 196, 10247-10253, **2002**.

Djikaev, Y. S., "Effect of the Surface-Stimulated Mode on the Kinetics of Homogeneous Crystal Nucleation in Droplets", *Journal of Physical Chemistry A*, 112, 6592-6600, **2008**.

Duft, D. and Leisner, T., "Laboratory evidence for volume-dominated nucleation of ice in supercooled water microdroplets", *Atmospheric Chemistry and Physics*, 4, 1997-2000, **2004**.

Durant, A. J., and Shaw, R. A., "Evaporation freezing by contact nucleation inside-out", *Geophysical Research Letters*, 32, L20814, **2005**.

Hartung, W. H. and Avedisian, C. T., "On the electrodynamic balance", *Proceedings of the Royal Society of London*, 437, 237-266, **1992**.

Held, I. M. and Soden, B. J., “Robust Responses of the Hydrological Cycle to Global Warming”, *Journal of Climate*, 19, 5686-5699, **2006**.

Hess, M., Koelemeijer, R. and Stammes P., “Scattering matrices of imperfect hexagonal ice crystals”, *Journal of Quantitative Spectroscopy and Radiative Transfer*, 60, 301-308, **1998**.

Hinds, W. C.,” Aerosol Technology: Properties, Behaviour and Measurement of Airborne Particles”, John Wiley and Sons, New York, **1999**.

Intergovernmental Panel on Climate Change, Climate Change 2007 - The Physical Science Basis: Contribution of Working Group I to the Fourth Assessment Report of the IPCC, Cambridge University Press, Cambridge, 2007.

Jackson, J. D. “Classical Electrodynamics”, John Wiley & Sons, Inc., New York, **1999**.

Karl T. R. and Trenberth, K. E., “Modern Global, Climate Change”, *Science*, 312, 1719-1723, **2003**.

Knopf, D. A., Koop, T., Luo, B. P., Weers, U. G. and Peter, T.: “Homogeneous nucleation of NAD and NAT in liquid stratospheric aerosols: insufficient to explain denitrification”, *Atmospheric Chemistry and Physics*, 2, 207–214, **2002**.

Koop, T., Lou, B., Tsias, A. and Peter T.: “Water activity as the determinant for homogeneous ice nucleation in aqueous solutions”, *Nature*, 406, 611, **2000**.

Liou K., -N., “Influence of Cirrus Clouds on Weather and Climate Processes: A Global Perspective”, *Monthly Weather Review*, 114, 1167-1199, **1986**.

Liou K., -N., ”An Introduction to Atmospheric Radiation”, Academic Press, Amsterdam, **2002**.

Lohmann, U. and Feichter, J., “Global indirect aerosol effects: a review”, *Atmospheric Chemistry and Physics*, 5, 715-737, **2005**.

Mishchenko, M. I., Travis, L. D. and Lacis, A. A.: “Scattering, Absorption, and Emission of Light by Small particles”, NASA Goddard Institute for Space Studies, New York, **2002**. Available at http://www.giss.nasa.gov/~crmin/books.html.

Olofson, K. F. G., Witt, G. and Pettersson, J. B. C., “Bistatic lidar measurements of clouds in the Nordic Arctic region”, *Applied Optics*, 47, 4777-4786, **2008**.

Omar, A. H. D., Winkler, D. and Won, J. G., “Aerosol models for the CALIPSO lidar inversion algorithm”, *SPIE*, 5240, 153-164, **2004**.

Pitter R. L. Pruppacher H. R., “A wind tunnel investigation of freezing of small water drops falling at terminal velocity in air”, *Quarterly Journal of the Royal Meteorological Society*, 99, 540550, **1973**.

Pruppacher H. R. and Klett J. D.: “Microphysics of Clouds and Precipitation”, Kluwer Academic

Publishers, 2nd Ed., Dordrecht, **1998**.

Roe, G. H. and Baker M. B.: "Why is climate sensitivity so unpredictable?", *Science*, 318, 629-632 , **2007**.

Salam, A., Lohmann, U., Crenna, B., Lesins, G., Klages, P., Rogers, D., Irani, R., MacGillivray, A. and Coffin, M., "Ice Nucleation Studies of Mineral Dust Particles with a New Continuous Flow Diffusion Chamber", *Aerosol Science and Technology*, 40, 134-143, **2006**.

Sigurbjörnsson, Ó. F. and Signorell, R., "Volume versus surface nucleation in freezing aerosols", *Physical Review E*, 77, 051601, **2008**.

Shaw, R. A., Durant A. J. and Mi, Y., "Heterogeneous Surface Crystallization Observed in Undercooled Water", *Journal of Physical Chemistry B*, 109, 9865-9868, **2005**.

Stetzer, O., Möhler, O., Wagner, R., Benz, S., Saathoff, H., Bunz, H. and Indris, O., "Homogeneous nucleation rates of nitric acid dihydrate (NAD) at simulated stratospheric conditions-part I: experimental results", *Atmospheric Chemistry and Physics*, 6, 3023–3033, **2006**.

Suzuki S., Nakajima A., Yoshida N., Sakai M., Hashimoto A., Kameshima Y. and Okada K., "Freezing of water droplets on silicon surfaces coated with various silanes", *Chemical Physics Letters*, 445, 37-41, **2007a**.

Suzuki, S., Nakajima, A., Yoshida, N., Sakai, M., Hashimoto, A., Kameshima, Y. and Okada, K., "Hydrophobicity and Freezing of a Water Droplet on Fluoroalkylsilane Coatings with Different Roughnesses", *Langmuir*, 23, 8674-8677, **2007b**.

Tabazadeh, A., Djikaev, Y. S., Hamill, P., and Reiss, H., "Laboratory Evidence for Surface Nucleation of Solid Polar Stratospheric Cloud Particles", *Journal of Physical Chemisry A*, 106, 10238-10246, **2002a**.

Tabazadeh, A., Djikaev, Y. S., and Reiss, H.: Surface crystallization of supercooled water in clouds, *Proceedings of the National Academies of Science USA*, 99, 15873-15878, **2002b**.

Weart, S., "The discovery of global warming", American Institute of Physics, **2007**. Available at http://www.aip.org/history/climate.

Zobrist, B., Marcolli, C., Koop, T., Luo, B. P., Murphy, D. M., Lohmann, U., Zardini, A. A., Krieger, U. K., Corti, T., Cziczo, D. J., Fueglistaler, S., Hudson, P. K., Thomson, D. S. and Peter, T., "Oxalic acid as a heterogeneous ice nucleus in the upper troposphere and its indirect aerosol effect", *Atmospheric Chemistry and. Physics*, 6, 3115-3129, 2006.